

MODAL ANALYSIS OF A HEAVY
TACTICAL WHEELED VEHICLE

by

Heather J. Molitoris

A submitted in partial fulfillment of the
requirements for the degree of

Masters of Engineering-Automotive
Engineering

University of Michigan-Ann Arbor

2007

Approved by _____
Faculty Supervisor

Approved by _____
Employer

Date _____

Report Documentation Page				Form Approved OMB No. 0704-0188	
Public reporting burden for the collection of information is estimated to average 1 hour per response, including the time for reviewing instructions, searching existing data sources, gathering and maintaining the data needed, and completing and reviewing the collection of information. Send comments regarding this burden estimate or any other aspect of this collection of information, including suggestions for reducing this burden, to Washington Headquarters Services, Directorate for Information Operations and Reports, 1215 Jefferson Davis Highway, Suite 1204, Arlington VA 22202-4302. Respondents should be aware that notwithstanding any other provision of law, no person shall be subject to a penalty for failing to comply with a collection of information if it does not display a currently valid OMB control number.					
1. REPORT DATE 10 DEC 2007		2. REPORT TYPE N/A		3. DATES COVERED -	
4. TITLE AND SUBTITLE Modal Analysis of a Heavy Tactical Wheeled Vehical				5a. CONTRACT NUMBER	
				5b. GRANT NUMBER	
				5c. PROGRAM ELEMENT NUMBER	
6. AUTHOR(S) Heather J. Molitoris				5d. PROJECT NUMBER	
				5e. TASK NUMBER	
				5f. WORK UNIT NUMBER	
7. PERFORMING ORGANIZATION NAME(S) AND ADDRESS(ES) US Army RDECOM-TARDEC 6501 E 11 Mile Rd Warren, MI 48397-5000, USA				8. PERFORMING ORGANIZATION REPORT NUMBER 18536	
9. SPONSORING/MONITORING AGENCY NAME(S) AND ADDRESS(ES) US Army RDECOM-TARDEC 6501 E 11 Mile Rd Warren, MI 48397-5000, USA				10. SPONSOR/MONITOR'S ACRONYM(S) TACOM/TARDEC	
				11. SPONSOR/MONITOR'S REPORT NUMBER(S) 18536	
12. DISTRIBUTION/AVAILABILITY STATEMENT Approved for public release, distribution unlimited					
13. SUPPLEMENTARY NOTES Submitted in partial fulfillment of the requirements for the degree of Masters of Engineering-Automotive Engineering University of Michigan-Ann Arbor, The original document contains color images.					
14. ABSTRACT					
15. SUBJECT TERMS					
16. SECURITY CLASSIFICATION OF:			17. LIMITATION OF ABSTRACT SAR	18. NUMBER OF PAGES 71	19a. NAME OF RESPONSIBLE PERSON
a. REPORT unclassified	b. ABSTRACT unclassified	c. THIS PAGE unclassified			

UNIVERSITY OF MICHIGAN

ABSTRACT

MODAL ANALYSIS OF A HEAVY TACTICAL WHEELED VEHICLE

by Heather J. Molitoris

Faculty Advisor: Dr. Nickolas Vlahopoulos
Employer: Calvin Kolp

The project's objectives are to model and simulate a heavy tactical wheeled vehicle with gross vehicle weight rating of 66,000 lbs, the Heavy Expanded Mobility Tactical Truck (HEMTT) M1120A4. Matlab will be used to complete a modal analysis of the half-truck model identifying the first 10 natural frequencies with corresponding mode shapes, the response of the cabin with input from the road, and the firing frequency of the selected engine. The analysis will consist of a baseline vehicle weight with a peacetime configuration and conclude with a parametric analysis of increasing the cabin weight, simulating the increased protection of the vehicle. The project goals will be to develop a detailed mathematical model of a heavy tactical wheeled vehicle. The detailed model will be used to complete a modal analysis identifying the fundamental vibration mode shapes and corresponding excitation frequencies which will be used to identify steering column and seat vibration impacts to the Soldier and crew.

The focus of this effort is to characterize and understand the impact of b-kit armor additions to the natural frequencies and mode shapes of a heavy tactical wheeled vehicle. The Army has identified a modular approach to protection identified as the Long Term Armor Strategy (LTAS) A-kit/B-kit approach. The LTAS A-Kit includes the automotive components of the vehicle and a baseline cab that incorporates the structural components for B-kit or increased protection components. The B-Kit would then consist of additional survivability technologies that can be applied to an A-Kit equipped vehicle in the field.

The mathematical model of the dynamic system will be used to approximate a particular frequency response function (FRF) to simulate the vibration characteristics of the cabin structure given the various inputs. The development of the mathematical model will approximate the system with lumped masses comprising the frame, wheel/tire assembly, powertrain, cabin, and flatbed. A sensitivity analysis of parameter variation will be performed to identify the critical parameters and limitations.

TABLE OF CONTENTS

List of Figures	ii
Glossary	iv
1.0 INTRODUCTION	3
2.0 APPROACH	4
2.1. SOURCE-PATH-RECEIVER MODEL	4
2.2. SYSTEM PROPERTIES	5
2.3. FRAME	8
2.4. Front and Rear Unsprung Mass	11
2.5. Crew Compartment	13
2.6. Powertrain	16
2.7. Truck Bed	17
2.8. SYSTEM MASS AND STIFFNESS MATRIX	19
2.9. Road Input	20
3.0 RESULTS	21
3.1. 10 PSF Solution	22
3.1.1. Mode Shapes	22
3.1.2. Powertrain Excitation	24
3.1.3. Road Excitation	25
3.1.4. Sensitivity Analysis	26
3.2. 20 PSF Solution	28
3.2.1. Mode Shapes	28
3.2.2. Powertrain Excitation	28
3.2.3. Road Excitation	29
3.3. 30 PSF Solution	29
3.3.1. Mode Shapes	29
3.3.2. Powertrain Excitation	30
3.3.3. Road Excitation	31
3.4. 40 PSF Solution	31
3.4.1. Mode Shapes	31
3.4.2. Powertrain Excitation	32
3.4.3. Road Excitation	32
3.5. 50 PSF Solution	33
3.5.1. Mode Shapes	33
3.5.2. Powertrain Excitation	33
3.5.3. Road Excitation	34
3.6. 60 PSF Solution	34
3.6.1. Mode Shapes	34
3.6.2. Powertrain Excitation	35
3.6.3. Road Excitation	36
3.6.4. Sensitivity Analysis	37
4.0 DISCUSSION	37
5.0 CONCLUSION	42
6.0 REFERENCES	43
Appendix A (Matlab Code)	44
Appendix B (Powertrain Description)	63

	List of figures	
<i>Number</i>		<i>Page</i>
Figure 1: HEMTT XM1120A4 Vehicle Dimension		6
Figure 2: Half Truck Model of the HEMTT XM1120 A4		7
Figure 3: C-Beam Dimension		8
Figure 4: Frame spacing between nodes		9
Figure 5: Cab Dimension		14
Figure 6: Vehicle Bounce		22
Figure 7: Vehicle Pitch		22
Figure 8: Front wheel hop		22
Figure 9: Front wheel hop		22
Figure 10: Frame Bending with Rear wheel hop		23
Figure 11: First frame bending		23
Figure 12: Frame bending with Cab out of phase		23
Figure 13: Frame bending with powertrain bounce		23
Figure 14: Frame Bending		23
Figure 15: Frame Bending		23
Figure 16: Idle Force Spectra		24
Figure 17: Steering column/Seat excitation with powertrain input at 10 PSF		24
Figure 18: Steering column/Seat excitation with powertrain input at maximum load at 10 PSF		25
Figure 19: Front and Rear tire input		25
Figure 20: Steering column/Seat Frequency Response Function at 10 PSF		26

Figure 21: 10 th Mode Shape excitation for case 1 and case 2 respectively	27
Figure 22: Steering column/Seat excitation with powertrain input at 20 PSF	29
Figure 23: Steering column/Seat Frequency Response Function at 20 PSF	29
Figure 24: Steering column/seat acceleration with powertrain input at 30 PSF	30
Figure 25: Steering column/Seat Frequency Response Function at 30 PSF	31
Figure 26: Steering column/seat acceleration with powertrain input at 40PSF	32
Figure 27: Steering column/Seat Frequency Response Function at 40 PSF	32
Figure 28: Steering column/seat acceleration with powertrain input at 50PSF	33
Figure 29: Steering column/Seat Frequency Response Function at 50 PSF	34
Figure 30: Steering column/seat acceleration with powertrain input at 60PSF	37
Figure 31: Steering column/Seat Frequency Response Function at 60 PSF	38
Figure 32: Noise, Vibration, and Harshness Sources in a vehicle [14]	39

GLOSSARY

Bode Plot: A plot of the frequency response function that includes log magnitude versus frequency plus phase versus frequency.

Degree of Freedom (DOF): The number of independent variables that must be specified to determine the state of a system.

Eigenvalues: The roots of the characteristic equation which indicate the natural frequency of the system in radians. To obtain the Natural frequency in Hz the roots must be multiplied by 180 and divided by 2π .

Eigenvectors: Used to determine the mode shape of the systems. The columns of the resulting matrix determine the displacement of each node or mass of the system when each frequency is excited.

Element Matrix Mapping: Is the mapping from element coordinates to global coordinates used in finite element analysis.

Finite Element Analysis: A computer-aided design technique for mathematically modeling a structure. Finite element modeling is used for structural analysis, heat transfer analysis, and modal analysis.

Forced Vibration: The oscillation of a system under the action of a forcing function.

Free Vibration: The oscillation of a system based on the system properties internal to the system without an excitation force.

Frequency Response Function: A representation of the path (H), with input force source (F) and output at a receiver (X). The FRF is shown as a function of frequency.

Modal Analysis: The study of the dynamic character of a system which is defined independently from the loads applied to the system and the response of the system.

Mode Shape: A representation of the deflection from nominal (no forcing function) of a system DOFs at the natural frequencies of the system.

Natural Frequency: The frequency at which an object will vibrate freely when set in motion.

Order: Multiples of the frequency obtained from periodic time data.

Path: The route that the time based function takes from the input source to the output receiver.

Receiver: Receiver represents quantitative and qualitative description of how the output energy is observed in the Source-Path-Receiver Model (SPR) model of the system.

Resonance: Resonance is the condition when the natural frequency of the system matches frequency of the applied forcing function. At resonance, it is the tendency of the system to oscillate with maximum amplitude.

Response: Output seen at the receiver in the Source-Path-Receiver Model.

Source: Source represents the quantitative and qualitative description of energy or force entering the system.

Source-Path-Receiver Model: Source-Path-Receiver model is an approach to solve NVH problems which involve identification of the source, path and receiver.

Transfer Path Analysis: Transfer Path Analysis is a method to study the combined response due to multiple sources acting through their corresponding paths. It assumes superposition principle, the sources can be coherent or uncorrelated and the paths depend on source input and receiver output degrees of freedom.

ACKNOWLEDGEMENT

The author wishes to thank Dr. Jim DeClerck, Wesley Bylsma, Dr. Nickolas Vlahopoulos, and Calvin Kolp for their assistance.

1. INTRODUCTION

Military vehicles are designed to operate in extreme conditions from off-road unimproved roads to primary highways, varying temperatures from minus 50 degrees Fahrenheit to 130 degrees Fahrenheit, and must be designed to account for varying configurations from peacetime to wartime mission essential configurations. The designers of military vehicles have to balance protection requirements with performance and payload needs while minimizing the logistics burden. A modal analysis of the system will describe the mechanical system in terms of its natural characteristics (frequency, damping, and mode shapes). The first order analysis will identify resonant frequencies of the system which vibration naturally occurs and understand the implications of those frequencies on the response of the structure and occupants (i.e. mode shapes) [1]. Mode shapes of the vibrating system identify critical properties of the system and should be considered a critical component during the design stage. It is known that inherent vibration modes in structural and mechanical support systems can shorten equipment life and cause premature failure. Designers of military vehicles must design for the maximum weight of the vehicle system which until recently for trucks was a standard automotive crew compartment configuration since tactical wheeled vehicles historically were never in the direct line of fire.

Since the war in Iraq, tactical wheeled vehicles have been up-armored to provide protection to our Soldiers in the asymmetric battlefield. The overall impact on the mechanical system as the Army continues to increase the crew compartment weight and protection is the issue being studied within this paper. The crew compartment weight will vary from a material solution of ten pounds per square foot (PSF) to sixty pounds per square foot. The intent is to understand the impact on the system especially on the crew compartment area with steering column excitation and seat excitation using the frequency response function. It should be noted that the material solutions identified will be varied parametrically from 10PSF to 60PSF and the material selected for the analysis is not the same material being fielded. The intent of this paper is to identify the trend of the system as the crew compartment weight increases and the impact not only to the crew, but the mode shapes of the system.

2. APPROACH

2.1. SOURCE-PATH-RECEIVER MODEL

The development of the model uses the frequency response function as outlined in the source-path-receiver (SPR) model commonly used in noise, vibrations, and harshness applications [2]. The source is the quantitative and qualitative description of energy or force entering the system. The path is defined as the mechanical mechanism that transmits to include the amplification, attenuation or delay of the energy from the source to the receiver. The receiver is defined as the quantitative a qualitative description of how the output energy is observed. The SPR model is commonly defined with the following equation:

$$\{X(w)\} = [H(w)] * \{F(w)\} \quad [1]$$

The sources for this model will be the powertrain and the road input. The path for the source will be defined with the frequency response function or $H(w)$. The powertrain will focus on the 3rd order engine firing during an idle condition. The road input will use a road profile acting through the tire patches when the vehicle travels at 45 MPH. The road input will be assumed to be linear and will neglect tire tread interaction.

The Transfer Path Analysis (TPA) will also be used within this analysis. TPA is a method to study the combined response due to multiple sources acting through their corresponding paths [2]. A TPA analysis has the following assumptions: assumes superposition; sources can be coherent or uncorrelated; paths depend on source input and receiver output DOFs [2]. TPA will be used to analyze the powertrain impact onto the Crew compartment and the road input onto the crew compartment area.

The system will require the principles of modal analysis and structural dynamics to analysis SPR. Modal analysis is required for the ability to study the dynamic character of a system which is defined independently from the loads applied to the system and the response of the system. This defines the system of interest which is a heavy duty truck that consists of a frame with masses attached to the frame. The modes of the system will correspond to

the natural frequencies of the system based on the weight and location of the lumped masses. The system will be assumed to be an undamped system. Eigenvalues will be used to determine the natural frequencies and Eigenvectors will be used to determine the mode shapes of the system. Eigenvalues are defined to be a set of scalars that associate a linear system of equations used within stability analysis and small oscillations of vibrating systems [3]. The system is considered to be a multiple degree of freedom (mDOF) Eigenvalue problem with the homogeneous undamped systems defined as:

$$[[K] - \lambda[M]]\bar{X}(w) = \bar{0} \quad [2]$$

where

K is the stiffness matrix of the system;

M is the mass matrix of the system;

λ is the eigenvalue, defined as the square of the natural frequencies for undamped systems;

and $X(w)$ is the response of the system.

The most critical aspect of the analysis is the characterization of the system. The SPR and TPA analysis requires mass and stiffness properties of every DOF defined within the system. The following sections with the approach will detail each significant component of the system with the modeling assumptions and applicable theory detailed. The critical components are the frame, front/rear suspension, crew compartment, powertrain, and truck bed with a section devoted to a generalized overview of the system. It should be understood that only public access information was used for this analysis.

2.2. SYSTEM PROPERTIES

The Heavy Expandable Mobility Tactical Truck-Load Handling System (HEMTT LHS) was analyzed. The variant of Oshkosh's HEMTT-LHS was the 8x8 XM1120A4 with a gross vehicle weight rating of 66,000 pounds and a gross combined weight rating of 100,000 pounds (Figure 1). The system was modeled with a standard crew configuration.

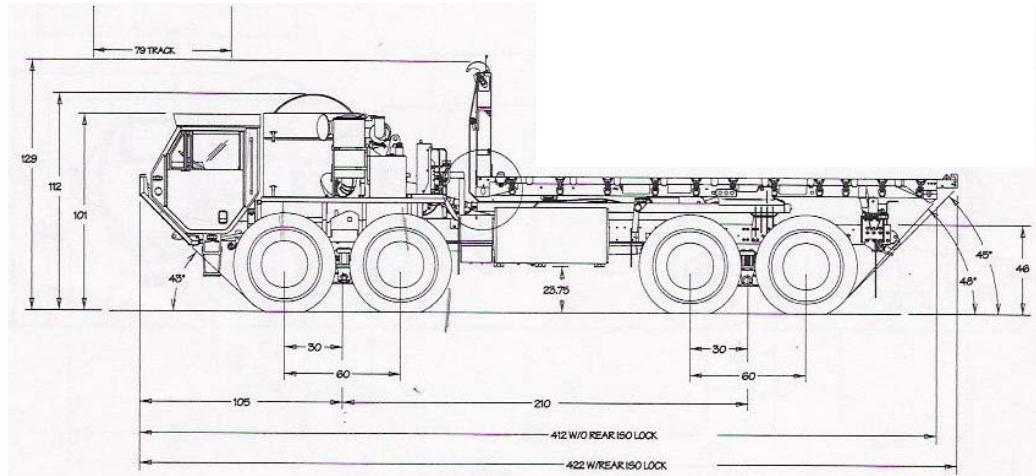


Figure 1: HEMTT XM1120A4 Vehicle Dimension

The system is divided into 9 lumped masses with 30 degrees of freedom (Figure 2). The analysis of this system consisted of treating the frame separately from the lumped masses in the initial analysis. An FEA analysis was used to define the spring and mass characteristics of the frame. The technique of matrix mapping was used to connect the lumped masses and springs to the frame. The lumped masses consist of the front and rear unsprung mass, crew compartment consisting of two masses, powertrain (engine, transmission, cooling system), and truck bed (three mass elements). The curb weight of the system is 35,500 lbs with a length of 412 inches, width of 96 inches, and height of 129 inches. The damping of the system is assumed to be

$$C = 0.0001 * K + 0.05 * M \quad [2b]$$

where K is the spring matrix and M is the mass matrix.

The nodal spacing of the frame was determined by lumping the masses and assuming connection points based on Figure 1. The crew compartment (CC) area connects to nodes 1, 2 and 3, 4 with the distance between identified as the width of the CC. The unsprung mass of the front suspension connects to nodes 5, 6 and 9, 10 of the frame with the distance between the two identified as the distance between the center of the hubs (Figure 1). The powertrain is connected to node 7, 8 of the frame and assumed to be located between the centers of the walking beam suspension. The truck bed is connected at three

points along the frame, nodes 11, 12; 15, 16; and 21, 22. The unsprung mass of the rear suspension connects to nodes 17, 18 and 19, 20 of the frame. Once again, the distance between the nodes identified as the distance between the centers of the hubs.

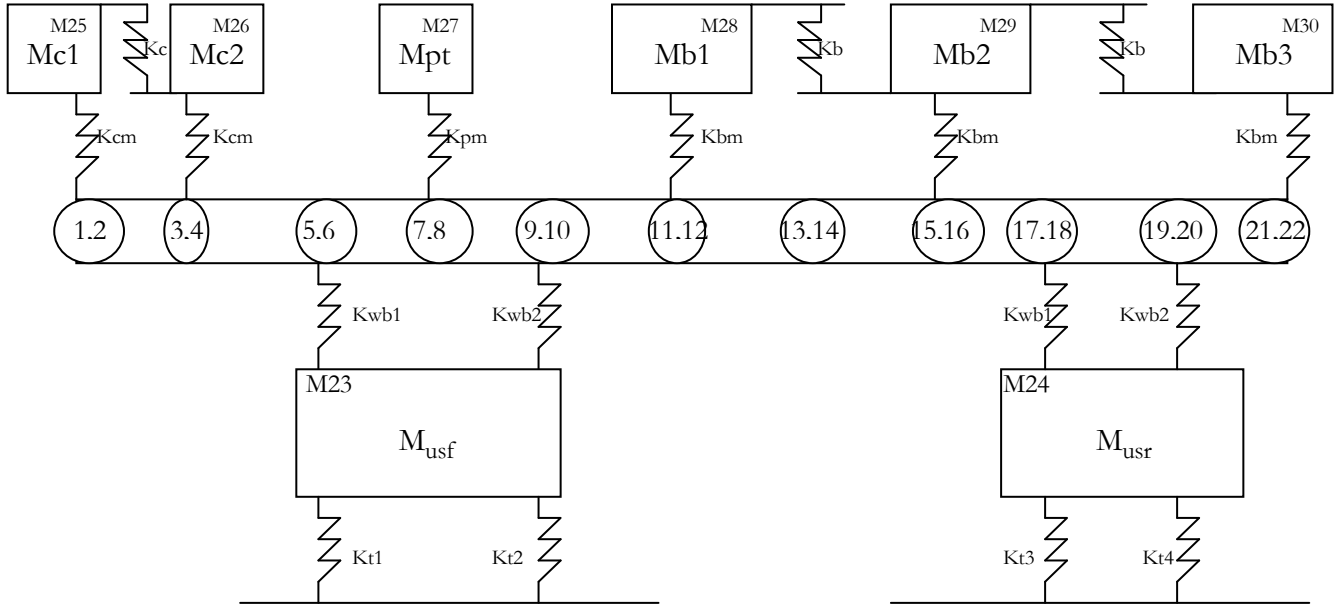


Figure 2: Half Truck Model of the HEMTT XM1120 A4

The crew compartment mass was the parameter that was varied to address the impact of adding additional b-armor kit weights. The parametric analysis assumed that the a-kit cab (peacetime configuration) was approximately 10 psf as the base structure. The weight was increased by 10 psf for six measurements which will provide enough data points for a trend analysis. The automotive weight of the system was primarily grouped into the bed of the vehicle with the exception of the unsprung weight which will be detailed in the following section. The sensitivity analysis will be completed using the error associated with each measurement. All mass parameters were given $\pm 5\%$, structural connection springs were given $\pm 0.5\%$ error, tire springs were given $\pm 20\%$, and springs connecting the lumped masses to the frame were given $\pm 15\%$.

Table 1: System Properties of the half truck model

	Minimum	Nominal	Maximum
Frame			
El (kN-m ²) $\pm 0.1\%$	1.294E+07	1.307E+07	1.320E+07
ρA (kg/m) $\pm 5\%$	76.003	80.004	84.004
Powertrain			
Mpt (kg) $\pm 5\%$	2193.346	2308.785	2424.224
Kpm (kN/m) $\pm 15\%$	2.069E+04	2.435E+04	2.800E+04
Suspension			
Musf (kg) $\pm 5\%$	2222.820	2339.811	2340.861
kt1 (kN/m) $\pm 20\%$	1.313E+03	1.641E+03	1.969E+03
kt2 (kN/m) $\pm 20\%$	1.313E+03	1.641E+03	1.969E+03
kwb1 (kN/m) $\pm 15\%$	9.825E+01	1.156E+02	1.329E+02
kwb2 (kN/m) $\pm 15\%$	9.825E+01	1.156E+02	1.329E+02
Musr (kg) $\pm 5\%$	2222.820	2339.811	2456.802
kt3 (kN/m) $\pm 20\%$	1.313E+03	1.641E+03	1.969E+03
kt4 (kN/m) $\pm 20\%$	1.313E+03	1.641E+03	1.969E+03
Truck Bed			
Mb1 (kg) $\pm 5\%$	3561.835	3749.301	3936.766
Mb2 (kg) $\pm 5\%$	1580.477	1663.660	1746.843
Mb3 (kg) $\pm 5\%$	1580.477	1663.660	1746.843
Kb (kN/m) $\pm 0.5\%$	4.123E+04	4.143E+04	4.164E+04
kbm (kN/m) $\pm 15\%$	6.458E+05	7.597E+05	8.737E+05

	Minimum	Nominal	Maximum
Truck Cab			
Kcm (kN/m) $\pm 15\%$	7.798E+04	9.175E+04	1.055E+05
10 PSF			
Mc1 (kg) $\pm 5\%$	665.006	700.006	735.007
Mc2 (kg) $\pm 5\%$	665.006	700.006	735.007
Kc (kN/m) $\pm 0.5\%$	1.284E+06	1.291E+06	1.297E+06
20 PSF			
Mc1 (kg) $\pm 5\%$	899.099	946.420	993.742
Mc2 (kg) $\pm 5\%$	899.099	946.420	993.742
Kc (kN/m) $\pm 0.5\%$	2.569E+06	2.582E+06	2.595E+06
30 PSF			
Mc1 (kg) $\pm 5\%$	1133.193	1192.835	1252.476
Mc2 (kg) $\pm 5\%$	1133.193	1192.835	1252.476
Kc (kN/m) $\pm 0.5\%$	3.661E+06	3.854E+06	3.873E+06
40 PSF			
Mc1 (kg) $\pm 5\%$	1367.286	1439.249	1511.211
Mc2 (kg) $\pm 5\%$	1367.286	1439.249	1511.211
Kc (kN/m) $\pm 0.5\%$	5.119E+06	5.145E+06	5.170E+06
50 PSF			
Mc1 (kg) $\pm 5\%$	1601.380	1685.663	1769.946
Mc2 (kg) $\pm 5\%$	1601.380	1685.663	1769.946
Kc (kN/m) $\pm 0.5\%$	6.403E+06	6.435E+06	6.468E+06
60 PSF			
Mc1 (kg) $\pm 5\%$	1835.473	1932.077	2028.681
Mc2 (kg) $\pm 5\%$	1835.473	1932.077	2028.681
Kc (kN/m) $\pm 0.5\%$	7.688E+06	7.726E+06	7.765E+06

2.3.FRAME

The frame of the HEMTT is 412 inches in length and characterized by 10 elements and 11 nodes. The beam is assumed to be a steel alloy with modulus of elasticity of (E) to be 30×10^6 PSI and a unit weight (ρ) of 0.28 lb/in^3 . The frame was modeled as two C-beam with a uniform cross section (Figure 3).

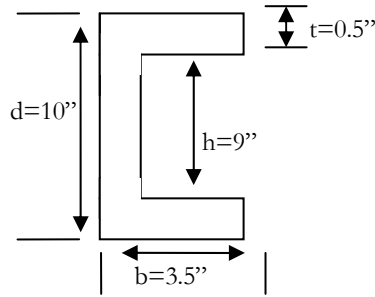


Figure 3: C-Beam Dimension

The area of the beam is determined with the following equation:

$$A = b * d - h(b - t) = 3.5 * 10 - ((10 - 2 * 0.5) - 0.5) = 8 \text{ in}^2 \quad [3]$$

The mass of the beam is defined to be:

$$M_{frame} = \rho A * L = 0.28 \frac{\text{lb}}{\text{in}^3} * 2 * 8 \text{ in}^2 * 412 \text{ in} = 1845.76 \text{ lbs} \quad [4]$$

The moment of inertia is defined to be:

$$I_{yc} = \frac{2*t*b^3 + ht^3}{3} - A*C_x^2 = \frac{2*0.5*3.5^3 + 9*0.5^3}{3} - 8(0.90625)^2 = 8.7123in^4 \quad [5]$$

The node spacing is defined as follows:

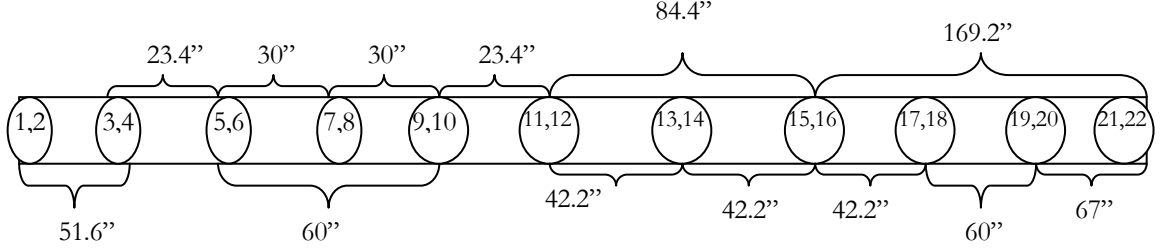


Figure 4: Frame spacing between nodes

The elements consisted of 4 DOF, to include the translation and rotation of each node.

The total element size was 10 with 11 nodes, for a total of 22 DOF associated with the frame. The elements were defined to be of lengths listed in Figure 4. The below matrix defines each element's associated stiffness:

$$[k_i] = \begin{Bmatrix} F_{1y} \\ M_1 \\ F_{2y} \\ M_2 \end{Bmatrix} = \frac{EI}{l_i^3} \begin{bmatrix} 12 & 6l_i & -12 & 6l_i \\ 6l_i & 4l_i^2 & -6l_i & 2l_i^2 \\ -12 & -6l_i & 12 & -6l_i \\ 6l_i & 2l_i^2 & -6l_i & 4l_i^2 \end{bmatrix} \begin{Bmatrix} u_{1y} \\ \theta_1 \\ u_{2y} \\ \theta_2 \end{Bmatrix} \quad [6]$$

The mass matrix is defined as the following:

$$[M_i] = \begin{Bmatrix} F_{1y} \\ M_1 \\ F_{2y} \\ M_2 \end{Bmatrix} = \frac{\rho A l_i}{420} \begin{bmatrix} 156 & 22l_i & 54 & -13l_i \\ 22l_i & 4l_i^2 & 13l_i & -3l_i^2 \\ 54 & 13l_i & 156 & -22l_i \\ -13l_i & -3l_i^2 & -22l_i & 4l_i^2 \end{bmatrix} \begin{Bmatrix} \ddot{u}_{1y} \\ \ddot{\theta}_1 \\ \ddot{u}_{2y} \\ \ddot{\theta}_2 \end{Bmatrix} \quad [7]$$

The element matrix mapping was defined for each element consisting of 4 rows corresponding to the 4 elemental DOF and 22 columns corresponding to the global DOFs for the beam. The matrix consists of the numerical value of 1 in the locations that correspond to the element coordinate mapping to the global coordinate system. For the 4th element, the corresponding element mapping matrix is defined as:

$$[T_4] = \begin{bmatrix} 0 & 0 & 0 & 0 & 0 & 0 & 1 & 0 & 0 & 0 & 0 & 0 & 0 & 0 & 0 & 0 & 0 & 0 & 0 & 0 & 0 \\ 0 & 0 & 0 & 0 & 0 & 0 & 0 & 1 & 0 & 0 & 0 & 0 & 0 & 0 & 0 & 0 & 0 & 0 & 0 & 0 & 0 \\ 0 & 0 & 0 & 0 & 0 & 0 & 0 & 0 & 1 & 0 & 0 & 0 & 0 & 0 & 0 & 0 & 0 & 0 & 0 & 0 & 0 \\ 0 & 0 & 0 & 0 & 0 & 0 & 0 & 0 & 0 & 1 & 0 & 0 & 0 & 0 & 0 & 0 & 0 & 0 & 0 & 0 & 0 \end{bmatrix} \quad [8]$$

A total of 10 element mapping matrices were developed to map the mass and stiffness properties to each element and global coordinate system. To map the stiffness matrix, the following equation was used:

$$[K_i] = [T_i]^T * [k_i] * [T_i] \quad [9]$$

where

i corresponds to the element number;

K is the stiffness matrix; and

T is the transfer matrix.

The defined stiffness of the entire uniform beam is defined by adding each stiffness element of the system or taking the summation of each element:

$$[K] = \sum_{i=1}^{10} K_i \quad [10]$$

To map the mass matrix, equation 9 and 10 are applied using the mass matrix definitions.

The beam's stiffness and mass matrices are 22 by 22 matrices. It is necessary to expand the matrices to complete the system DOF of 30 by 30 by adding 8 vertical columns and 8 rows at the end of the mass and stiffness matrices. The 8 x 8 addition at the end of the frame mass and stiffness matrices correspond to the 8 additional DOF which will be defined within this section. It should be noted that the method described above distributes the mass properties across each element so they are not lumped at the nodal points. The lumped masses or DOFs 23 through 30 do not have this characteristic and will be diagonal for the spring and mass matrices. The final component of the frame, is mapping the DOF for the lumped masses to the DOF of the frame through the spring parameters as defined in Table 1.

The springs connecting the translational nodes to the lumped masses are critical to understand the behavior of the system. The Matlab code listed in Appendix A will detail the process, an example will be provided to illustrate the analysis. Figure 2 identifies that DOF 1 is connected to DOF 25, the following matrices were used to model that connection. Equation 8 is necessary to map the element DOF to the global coordinate system. Equation 8 indicates that a mapping matrix and spring matrix must be defined. In the case of DOF 1 to DOF25, the following spring and mapping matrices are required:

$$[T_{1-25}] = \begin{bmatrix} 1 & 0 \\ 0 & 0 \\ 0 & 0 \end{bmatrix} \quad [11]$$

Note that the value 1 is placed connecting element DOF 1 to global DOF 1 and element DOF 25 to global DOF 25.

For each of the additional DOFs, equation 12 was completed to obtain the half truck model stiffness matrix.

$$[K_{cm}] = \begin{bmatrix} k_{cm} & -k_{cm} \\ -k_{cm} & k_{cm} \end{bmatrix} \quad [12]$$

Where

K_{cm} is the stiffness of the spring connecting the crew compartment to the frame.

The mapping of the additional lumped masses used equation 11 to add the additional contribution of the springs. The final step to determine the stiffness of the complete system was to add the stiffness from the frame to the stiffness from the springs connecting the lumped masses to the frame to define the stiffness of the system.

2.4. Front and Rear Unsprung Mass

The unsprung mass will consist of the suspension, tire-wheel assembly, axles, brake, and steering components of the system. The connection point to the frame of the unsprung mass are located at the center of the wheel-tire assembly. Tire damping will be neglected

based on the research presented by Heo published by the Journal of Vibration and Acoustics [1]. The front unsprung mass configuration consists of 2 suspension systems, 4 tires, and 2 axles.

The HEMTT uses the Hendrickson RT340 with equalizing beam for the front suspension. The springs denoted to be k_{wb1} and k_{wb2} in figure 2 are in parallel which defines the spring equivalent to be:

$$k_{eq} = k_{wb1} + k_{wb2} \quad [13]$$

The spring rate or spring equivalent of the walking beam was determined via the manufacturer to be 660 lb_f/in (115.58 kN/m) or 330 lb_f/in for k_{wb1} and k_{wb2} . It is critical to note that the half truck model accounts for the complete system weight so k_{wb1} and k_{wb2} will be modeled at twice k_{wb1} to account for the front combined suspension. The installed weight of the suspension system is 1,199 lbs per unit.

The tire is defined as the Michelin with tubes 16.00 R20 XZL. The tire specifications were found on Michelin's website and load range G was used since it corresponded to the max vehicle speed. The tire weight was listed to be 219.4 pounds. The tire stiffness was determined based on the information listed in the specification. The unloaded radius of the tire is 23.4 inches and the loaded radius of the tire is 21.4 inches. The maximum tire load for a single tire is 9370 pounds. The stiff was determined with the following equation:

$$F = k * \Delta x \quad [14]$$

where

F is the maximum tire load (9370 pounds); and

Δx is the difference between the loaded and unloaded radius to give:

$$k = \frac{F}{\Delta x} = \frac{9370}{23.4 - 21.4} = 4685 lb_f / in = 820.5 kN / m \quad [15]$$

The axle weight was determined with the following equation:

$$W_{axle} = \rho * A * L \quad [16]$$

where

ρ is the unit mass of the system assumed to be steel alloy A36 with a unit mass of 0.283 lbm/in³;

A to be the area of the axle or πr^2 ; and

L to be the length of the axle defined to be 96 inches.

The weight of the axle is 341.40 pounds. The HEMTT has two axles per suspension components for a total of 6 axles.

The wheel, steering, and braking components were assumed to have weight of 300 pounds. The final assumption for the unsprung mass is that the front and rear have the same components so the above analysis is used to determine the unsprung mass of the rear and spring characteristics for the walking beams and tires. Table 2 lists the weights and total unsprung mass considered for the front and rear.

Table 2: Front Unsprung Mass

Component	Weight (lbs)	Amount	Total (lbs)
Suspension	1199.00	2	2398.00
Axle	341.40	2	682.80
Tire	219.40	4	877.60
Wheel/Brake/Steering	300.00	4	1200.00
Total Unsprung Mass (lbs):			5158.4
Total Unsprung Mass (kg):			2339.811

2.5. Crew Compartment

The crew compartment is the parameter that is being varied to study the impact of b-armor kit weight on the system. The cab is assumed to be constructed of rectangles neglecting any difference in the opaque and transparent armor which for this analysis are assumed to be homogeneous. Figure 5 shows the cab dimensions.

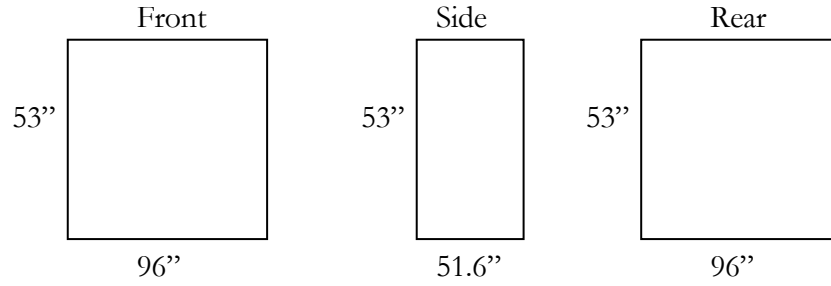


Figure 5: Cab Dimension

The total area of the system is defined to be:

$$A_T = A_F + 2 * A_s + A_R \quad [17]$$

where A is the area defined to be L*h for each section identified in Figure 5.

The above equation is used to determine the mass of the system based on the identified pounds per square foot listed in Table 3. The PSF multiplied by the area of the system will provide the crew compartment mass. An additional 2000 pounds was added to the crew compartment mass to account for the seats, instrument panel, steering wheel and additional standard equipment within the compartment.

The thickness of the material solution was determined with the following equation:

$$t = \frac{PSF}{\rho} = \frac{\frac{PSF}{12^2}}{\rho} = \frac{PSF}{12^2 \rho} \quad [18]$$

where

t is the thickness;

PSF is the pounds per square foot with 12² converting feet to inches; and

ρ is the mass unit weight of the AL Alloy 7075 defined to be 0.101 lbm/in³.

The crew compartment mass was equally divided into two components the mass to simulate the cabin bounce and pitching. The mass and thickness were needed to calculate the stiffness parameter (k_c) between the crew compartments. The assumption was made

that the stiffness of the frame is comparable to the stiffness of a rectangular plane. This assumption will allow the model to account for the varying thickness of the material, but will not account for the hollowed structural integrity of the cabin area. Ideally, an FEA solver should be used to analyze this system, but as a first order model the assumption will hold true. The stiffness equation is defined to be:

$$K_c = \frac{A * E}{L} \quad [19]$$

where

K_c is the stiffness of the cab element;

A is the area defined to be height times thickness;

E is the modulus of elasticity for AL Alloy 7075 defined to be 10.4×10^6 PSI; and

L is defined to be the length which is 51.6 inches.

Table 3: Crew Compartment derived properties

PSF	Mass (lbs)	Mass (kg)	Thickness (in)	K_c (lbf/in)
10	3086.50	1400.013	0.688	7.345E+06
20	4173.00	1892.841	1.375	1.469E+07
30	5259.50	2385.669	2.063	2.203E+07
40	6346.00	2878.497	2.750	2.938E+07
50	7432.50	3371.325	3.438	3.672E+07
60	8519.00	3864.153	4.125	4.407E+07

The last parameter solved for the crew compartment was the attachment points of the crew compartment to the frame. The assumption used that the designers would attempt to select the bushing that minimized the crew compartment movement when subjected to the maximum cabin load onto the system, identified as the 60 PSF solutions. Equation 14 above is applied such that:

$$k_{cm} = \frac{F_{Cab}}{\Delta x} = \frac{6519.99 * 32.14}{0.1} = 2.0955247 * 10^6 \text{ lb}_f / \text{ft} \quad [20]$$

where

k_{cm} is the stiffness of the bushing connecting the crew compartment to the frame;

F_{cab} is the maximum weight (60 PSF) multiplied by the gravity constant; and Δx is an assumed displacement between the crew compartment and the frame defined to be 0.1 feet.

Equation 11 would be used to determine the contribution of the individual connection points to the equivalent k_{cm} . Therefore k_{cm} is divided by four to determine the individual k_{cm} values.

2.6. Powertrain

The powertrain consists of the engine, transmission and cooling system. The engine is defined to be the Caterpillar C15 15.2L diesel engine. It is an in-line 6 that is positioned directly behind the crew compartment and weights 3090 pounds (Appendix B). The transmission is an Allison HT740, which is a 4-speed automatic. The combined weight of the transmission and cooling system is assumed to be 2000 pounds. The mass of the powertrain is defined to be 5,090 pounds. The attachment point of the engine to the frame assumes a small deflection and applies equation 18 above substituting the mass of the powertrain in for the mass of the crew compartment to determine k_{pm} such that:

$$k_{pm} = \frac{5090 * 32.14}{0.1} = 1.6359260 * 10^6 lb_f / ft \quad [21]$$

Note that the stiffness of the spring is less than the stiffness of the crew compartment connection since the stiffness is derived from the weight applied this is appropriate.

The powertrain excitation was derived based on the firing frequency of the inline 6 cylinder diesels. The firing frequency is defined to be:

$$FF(Hz) = \frac{RPM}{60} * Engine_Order \quad [22]$$

where Engine order is defined to be:

$$EngineOrder = \frac{No_of_Cylinders}{2} \quad [23]$$

The idle of the HEMTT XM1120 is assumed to be 900 RPMs. Therefore, the firing frequency for the HEMTT system is defined to be:

$$FF(HEMTT) = \frac{900}{60} * 3 = 45Hz \quad [24]$$

The idle force spectra for the powertrain excitation was developed using the given equation:

$$|F_p| = 10 * (1 - .1 * (FF - freq)^2) \quad [25]$$

Equation 25 filters the excitation to peak at the 45Hz excitation frequency, but uses an inverse parabolic impulse excitation instead of an impulse function at 45 Hz.

2.7. Truck Bed

The truck bed as mentioned previously accounted for the additional automotive weight of the HEMTT system to include the crane, diesel fuel, and structural support required for securing ISO containers and other cargo items. The method used the curb weight identified to be 35,500 lbs and then subtracted the engine, unsprung mass (front and rear), frame, and the crew compartment to derived the truck bed weight.

Table 4: Truck Bed weight

		PSF 10 (kg)
Unsprung		2339.811
Frame		837.220
Powertrain		2308.785
Crew Compartment		3086.500
Bed	M _{b1}	3609.764
	M _{b2}	1524.123
	M _{b3}	1524.123
	Total	6658.011

The bed lumped mass structure is divided into three components, the front which houses the crane, diesel fuel and motor to operate the crane; the middle and rear which are the structural support for the cargo. To divide the mass appropriately to the components, the following formula was used:

$$M_{bed} = mass_{bed} - m_{dieselfuel} - m_{crane} \quad [27]$$

The mass of the bed was explained above and is listed in Table 4. The mass of the diesel fuel was found by multiplying the density of diesel fuel (7.09 lb/gal) by the fuel tank capacity of the system (155 gallons) for a total mass of 1,098.95 pounds. The mass of the crane was assumed to be approximately 2,500 pounds plus an additional 1000 pounds for cabling and a motor. The crane was assumed to be a grove crane for a load handling system. The M_{bed} was divided by 3, corresponding to the number of lumped masses for the truck bed, to define the distributed weight across all three lumped parameters. The first part of the bed, m_{b1} was defined as follows:

$$m_{b1} = M_{bed} + m_{dieselfuel} + m_{crane} \quad [28]$$

The stiffness between the truck bed masses is assumed to be a rectangular beam main of steel alloy with a defined Modulus of Elasticity of 30×10^6 PSI and a density of 0.28 lb/in³. Equation 19 was used to determine the stiffness between the lumped masses such that:

$$k_b = \frac{AE}{L} = \frac{(4 * .5) * 30 \times 10^6}{253.6} = 0.23659 * 10^6 lb_f / in \quad [29]$$

The stiffness of the spring that connects the bed to the frame is derived using the gross combined weight rating of 100,000 pounds of which 80,985.42 pounds is assumed to be located in the bed. The 80,985.42 pounds is derived using the process outlined in Table 4. Equation 20 is applied in order to determine the stiffness such that:

$$k_{bm} = \frac{F}{\Delta x} = \frac{80985.42 * 32.14}{0.1} = 260.287 * 10^5 lb_f / in \quad [30]$$

The bed is assumed to attach to the frame in three equivalent connection points such that Equation 13 is applicable and thus the stiffness equivalent for k_{bm1} , k_{bm2} , and k_{bm3} is:

$$k_{bm1} = k_{bm2} = k_{bm3} = \frac{k_{bm}}{3} = \frac{260.287 * 10^5}{3} = 86.7624 * 10^5 lb_f / in \quad [31]$$

The system parameters are listed in Table 1 with the main difference being all system parameters were converted from English units to metric units for the Matlab model.

2.8. SYSTEM MASS AND STIFFNESS MATRIX

The mass and stiffness matrices were created in Matlab using the matrix mapping technique [2]. The six different mass and stiffness matrices were developed using the parameters identified in Table 1 for the mass and stiffness changes based on the crew compartment weight for the 10 through 60 PSF solutions. The mass matrix has the characteristic distribution of the mass properties across elements one through twenty-two corresponding to the frame. This is an attempt in the FEA model to distribute the mass properties across each element so they are not lumped at the nodal points. The lumped masses or DOFs twenty-three through thirty do not have this characteristic and are diagonal. The Matlab program contains six mass matrixes with DOF twenty-five and DOF twenty-six changed to reflect the crew compartment additions.

Table 5: Mass Matrix for the 10 PSF HEMTT Solution

	DOF 1	DOF 2	DOF 3	DOF 4	DOF 5	DOF 6	DOF 7	DOF 8	DOF 9	DOF 10	DOF 11	DOF 12	DOF 13	DOF 14	DOF 15	DOF 16	DOF 17	DOF 18	DOF 19	DOF 20	DOF 21	DOF 22	DOF 23	DOF 24	DOF 25	DOF 26	DOF 27	DOF 28	DOF 29	DOF 30
DOF 1	0.473	3.595	0.129	-2.129	0	0	0	0	0	0	0	0	0	0	0	0	0	0	0	0	0	0	0	0	0	0	0	0	0	0
DOF 2	3.595	0.8577	2.129	-2.842	0	0	0	0	0	0	0	0	0	0	0	0	0	0	0	0	0	0	0	0	0	0	0	0	0	0
DOF 3	0.129	2.129	28.304	-2.859	0.569	-0.4374	0	0	0	0	0	0	0	0	0	0	0	0	0	0	0	0	0	0	0	0	0	0	0	0
DOF 4	-2.129	-2.842	-2.859	0.8077	0.4374	-0.0599	0	0	0	0	0	0	0	0	0	0	0	0	0	0	0	0	0	0	0	0	0	0	0	0
DOF 5	0	0	0.569	0.4374	20.153	0.4764	3.9191	-0.71893	0	0	0	0	0	0	0	0	0	0	0	0	0	0	0	0	0	0	0	0	0	0
DOF 6	0	0	-0.4374	-0.0599	0.4764	0.24855	0.71893	-0.12642	0	0	0	0	0	0	0	0	0	0	0	0	0	0	0	0	0	0	0	0	0	0
DOF 7	0	0	0	0	3.9191	0.71893	22.643	0	3.9191	-0.71893	0	0	0	0	0	0	0	0	0	0	0	0	0	0	0	0	0	0	0	0
DOF 8	0	0	0	0	-0.71893	-0.12642	0	0.33712	0.71893	-0.12642	0	0	0	0	0	0	0	0	0	0	0	0	0	0	0	0	0	0	0	0
DOF 9	0	0	0	0	0	0	3.9191	0.71893	20.153	-0.4764	3.9589	-0.4374	0	0	0	0	0	0	0	0	0	0	0	0	0	0	0	0	0	0
DOF 10	0	0	0	0	0	0	0	-0.71893	-0.12642	-0.4764	0.24855	0.4374	-0.0599	0	0	0	0	0	0	0	0	0	0	0	0	0	0	0	0	0
DOF 11	0	0	0	0	0	0	0	3.9589	0.4374	24.757	1.8672	5.5128	-1.4226	0	0	0	0	0	0	0	0	0	0	0	0	0	0	0	0	0
DOF 12	0	0	0	0	0	0	0	-0.4374	-0.0599	1.8672	5.5128	1.4226	-0.35188	0	0	0	0	0	0	0	0	0	0	0	0	0	0	0	0	0
DOF 13	0	0	0	0	0	0	0	0	5.5128	1.4226	31.862	5.5128	-1.4226	0	0	0	0	0	0	0	0	0	0	0	0	0	0	0	0	0
DOF 14	0	0	0	0	0	0	0	0	-1.4226	-0.35188	0	0.63834	1.4226	-0.35188	0	0	0	0	0	0	0	0	0	0	0	0	0	0	0	0
DOF 15	0	0	0	0	0	0	0	0	5.5128	1.4226	31.862	5.5128	-1.4226	0	0	0	0	0	0	0	0	0	0	0	0	0	0	0	0	0
DOF 16	0	0	0	0	0	0	0	0	-1.4226	-0.35188	0	0.63834	1.4226	-0.35188	0	0	0	0	0	0	0	0	0	0	0	0	0	0	0	0
DOF 17	0	0	0	0	0	0	0	0	0	0	0	0	0	5.5128	1.4226	38.569	2.4502	7.8381	-2.8757	0	0	0	0	0	0	0	0	0	0	0
DOF 18	0	0	0	0	0	0	0	0	0	0	0	0	0	-1.4226	-0.35188	2.4502	1.8177	2.8757	-1.0114	0	0	0	0	0	0	0	0	0	0	0
DOF 19	0	0	0	0	0	0	0	0	0	0	0	0	0	7.8381	2.8757	47.925	1.2018	8.7528	-3.5859	0	0	0	0	0	0	0	0	0	0	0
DOF 20	0	0	0	0	0	0	0	0	0	0	0	0	0	-2.8757	-1.0114	1.2018	3.2262	3.5859	-1.4082	0	0	0	0	0	0	0	0	0	0	0
DOF 21	0	0	0	0	0	0	0	0	0	0	0	0	0	0	8.7528	3.5859	25.285	-6.0684	0	0	0	0	0	0	0	0	0	0	0	0
DOF 22	0	0	0	0	0	0	0	0	0	0	0	0	0	0	-3.5859	-1.4082	-6.0684	1.8777	0	0	0	0	0	0	0	0	0	0	0	0
DOF 23	0	0	0	0	0	0	0	0	0	0	0	0	0	0	0	0	0	0	0	2339.9	0	0	0	0	0	0	0	0	0	0
DOF 24	0	0	0	0	0	0	0	0	0	0	0	0	0	0	0	0	0	0	0	0	2339.9	0	0	0	0	0	0	0	0	0
DOF 25	0	0	0	0	0	0	0	0	0	0	0	0	0	0	0	0	0	0	0	0	0	700.01	0	0	0	0	0	0	0	0
DOF 26	0	0	0	0	0	0	0	0	0	0	0	0	0	0	0	0	0	0	0	0	0	0	700.01	0	0	0	0	0	0	0
DOF 27	0	0	0	0	0	0	0	0	0	0	0	0	0	0	0	0	0	0	0	0	0	0	0	2338.9	0	0	0	0	0	0
DOF 28	0	0	0	0	0	0	0	0	0	0	0	0	0	0	0	0	0	0	0	0	0	0	0	0	3748.3	0	0	0	0	0
DOF 29	0	0	0	0	0	0	0	0	0	0	0	0	0	0	0	0	0	0	0	0	0	0	0	0	0	0	1983.7	0	0	0
DOF 30	0	0	0	0	0	0	0	0	0	0	0	0	0	0	0	0	0	0	0	0	0	0	0	0	0	0	0	1983.7	0	0

The system's stiffness matrix connects the DOF with the frame and for the FEA analysis distributing the stiffness along the frame across the nodes one through twenty-two. The Matlab program contains six stiffness matrix with DOF twenty-five to DOF one and DOF twenty-six to DOF three connects changing based on the stiffness increased with the thickness of the crew compartment increasing.

Table 6: Stiffness Matrix for the 10 PSF HEMTT Solution

	DOF 1	DOF 2	DOF 3	DOF 4	DOF 5	DOF 6	DOF 7	DOF 8	DOF 9	DOF 10	DOF 11	DOF 12	DOF 13	DOF 14	DOF 15	DOF 16
DOF 1	9.97E+07	5.24E+06	-8.00E+06	5.24E+06	0	0	0	0	0	0	0	0	0	0	0	0
DOF 2	5.24E+06	4.58E+06	-5.24E+06	2.29E+06	0	0	0	0	0	0	0	0	0	0	0	0
DOF 3	-8.00E+06	-5.24E+06	1.85E+08	2.02E+07	-8.57E+07	2.55E+07	0	0	0	0	0	0	0	0	0	0
DOF 4	5.24E+06	2.29E+06	2.02E+07	1.47E+07	-2.55E+07	5.05E+06	0	0	0	0	0	0	0	0	0	0
DOF 5	0	0	-8.57E+07	-2.55E+07	1.27E+08	-9.98E+06	-4.07E+07	1.55E+07	0	0	0	0	0	0	0	0
DOF 6	0	0	2.55E+07	5.05E+06	-9.98E+06	1.80E+07	-1.55E+07	3.94E+06	0	0	0	0	0	0	0	0
DOF 7	0	0	0	0	-4.07E+07	-1.55E+07	1.06E+08	0	-4.07E+07	1.55E+07	0	0	0	0	0	0
DOF 8	0	0	0	0	1.55E+07	3.94E+06	0	1.58E+07	-1.55E+07	3.94E+06	0	0	0	0	0	0
DOF 9	0	0	0	0	0	0	-4.07E+07	-1.55E+07	1.27E+08	9.98E+06	-8.57E+07	2.55E+07	0	0	0	0
DOF 10	0	0	0	0	0	0	1.55E+07	3.94E+06	9.98E+06	1.80E+07	-2.55E+07	5.05E+06	0	0	0	0
DOF 11	0	0	0	0	0	0	0	-8.57E+07	-2.55E+07	8.60E+08	-1.76E+07	-1.46E+07	7.83E+06	0	0	0
DOF 12	0	0	0	0	0	0	0	2.55E+07	5.05E+06	-1.76E+07	1.57E+07	-7.83E+06	2.80E+06	0	0	0
DOF 13	0	0	0	0	0	0	0	0	0	-1.46E+07	-7.83E+06	2.92E+07	0	-1.46E+07	7.83E+06	0
DOF 14	0	0	0	0	0	0	0	0	0	7.83E+06	2.80E+06	0	1.12E+07	-7.83E+06	2.80E+06	0
DOF 15	0	0	0	0	0	0	0	0	0	0	-1.46E+07	-7.83E+06	7.89E+08	0	1.12E+07	0
DOF 16	0	0	0	0	0	0	0	0	0	0	7.83E+06	2.80E+06	0	0	0	1.12E+07
DOF 17	0	0	0	0	0	0	0	0	0	0	0	0	0	-1.46E+07	-7.83E+06	0
DOF 18	0	0	0	0	0	0	0	0	0	0	0	0	0	7.83E+06	2.80E+06	0
DOF 19	0	0	0	0	0	0	0	0	0	0	0	0	0	0	0	0
DOF 20	0	0	0	0	0	0	0	0	0	0	0	0	0	0	0	0
DOF 21	0	0	0	0	0	0	0	0	0	0	0	0	0	0	0	0
DOF 22	0	0	0	0	0	0	0	0	0	0	0	0	0	0	0	0
DOF 23	0	0	0	0	-1.16E+05	0	0	-1.16E+05	0	0	0	0	0	0	0	0
DOF 24	0	0	0	0	0	0	0	0	0	0	0	0	0	0	0	0
DOF 25	-9.18E+07	0	0	0	0	0	0	0	0	0	0	0	0	0	0	0
DOF 26	0	0	-9.18E+07	0	0	0	0	0	0	0	0	0	0	0	0	0
DOF 27	0	0	0	0	0	-2.43E+07	0	0	0	0	0	0	0	0	0	0
DOF 28	0	0	0	0	0	0	0	0	0	-7.60E+08	0	0	0	0	0	0
DOF 29	0	0	0	0	0	0	0	0	0	0	0	0	0	0	-7.60E+08	0
DOF 30	0	0	0	0	0	0	0	0	0	0	0	0	0	0	0	0

The mass and stiffness matrix define the complete system to determine the natural frequencies using eigenvalues.

2.9. Road Input

The road input transmits through the wheel center of the unsprung masses DOF twenty-three and DOF twenty-four. The spring force is doubled to account for two tires located on the unsprung masses and multiplied by two to account for the half-truck model. The magnitude and phase of the response at the steering column assumed to be DOF twenty-five and the seat DOF twenty-six due to the road profile acting through the tire patch (y9 and y10) when the truck travels at a speed of 72.4 kph (45 MPH). The truck has a wheelbase of 210 inches (5.334 meters). Equation 32 defines the linear spectrum of the road profile.

$$y(f) = \frac{1}{1000 \left(1 + \left(\frac{freq}{15} \right)^3 \right)} m \quad [32]$$

An assumption in the analysis was to combine k_{t1} and k_{t2} into one input onto DOF 23 or the front unsprung mass. Given that the truck is traveling at a constant speed of 72.4 kph and the wheelbase is defined to be 5.334 meters (210 inches), one can determine the linear spectrum of the road profile for inputs at y9 and y10. Where y9 corresponds to the front

suspension system and y10 corresponds to the rear suspension system. The time delay from when the front wheel of the vehicle encounters the road input versus the rear wheel is defined to be:

$$\Delta t = \frac{WheelBase}{Speed} = \frac{L}{|V|} = \frac{5.334m}{\frac{72.4 * 10}{36} m/s} = \frac{181}{9} \text{sec} \quad [33]$$

To translate that into the frequency domain:

$$\theta = 2\pi * freq * \Delta t \quad [34]$$

Delay is represented as:

$$Delay = Cos(\theta) - j * Sin(\theta) \quad [35]$$

For theta at position y9, the road input does not experience a delay and therefore the theta value is zero. For theta at the position y10, the delay is defined in equations 33, 34, and 35.

Therefore, the road profile or forcing function for the road input at location y9 and y10 are:

$$Y_9 = Y(f) * 1000 * (\cos(0) - j * \sin(0)) = Y(f) * 1000 \quad [36]$$

$$Y_{10} = Y(f) * 1000(Delay(\theta)) = Y(f) * 1000 * (Cos(\theta) - j * Sin(\theta)) \quad [37]$$

3. RESULTS

The results will be presented for each crew compartment weight class. The mode shapes will be provided for the 10 PSF weight and any mode shapes that differ significantly for the others; powertrain and the road excitation impact onto the crew compartment area will also be presented. The results will contain a sensitivity analysis of the system for the 10PSF and 60 PSF solution set by two cases: the first case is to vary all springs and masses to the maximum value; and the second is to vary the springs to the maximum value with the masses to the minimum values.

3.1. 10 PSF Solution

3.1.1. Mode Shapes

The mode shapes of the 10 PSF solution for the crew compartment are listed in figures six through fifteen. The vehicle pitch corresponds to the first natural frequency, it would appear that the crane dominates the bed weight with very little movement for the second and third lumped masses of the bed. This is assumed to be based on the nominal weight assigned to those lumped masses. The out of phase wheel hop for the front suspensions seem to be excited on the third and fourth natural frequency and eight natural frequency respectively. The in-phase rear wheel hop corresponds to the eighth natural frequency respectively. The powertrain

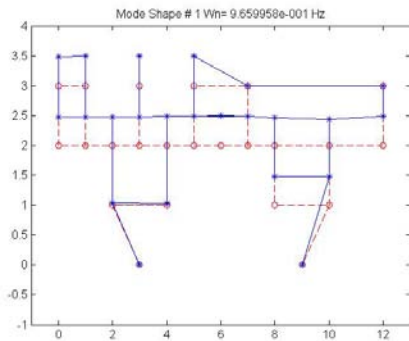


Figure 6: Vehicle Bounce

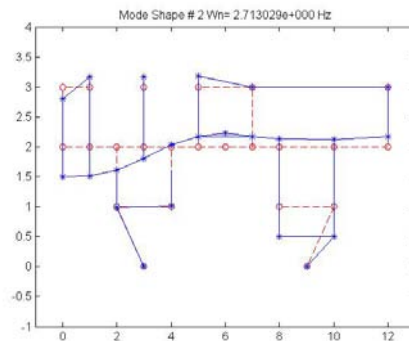


Figure 7: Vehicle Pitch

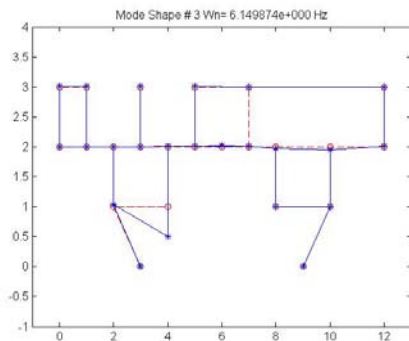


Figure 8: Front wheel hop

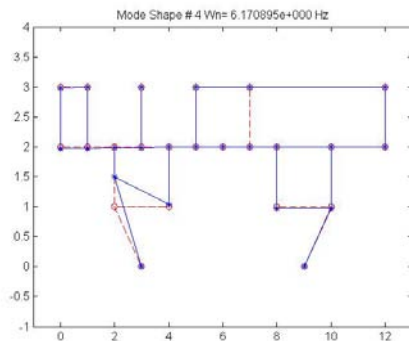


Figure 9: Front wheel hop

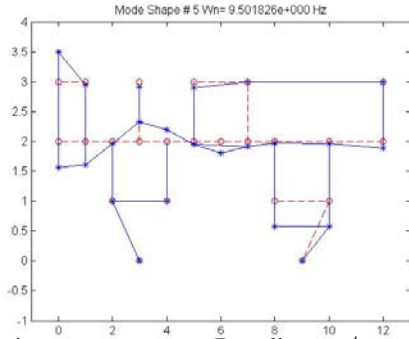


Figure 10: Frame Bending w/ Rear wheel hop

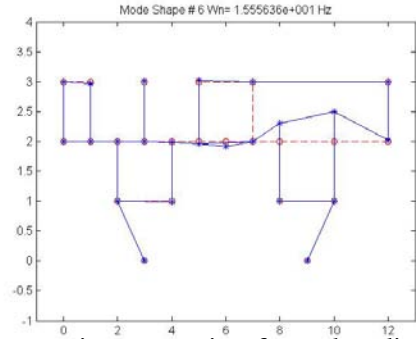


Figure 11: First frame bending

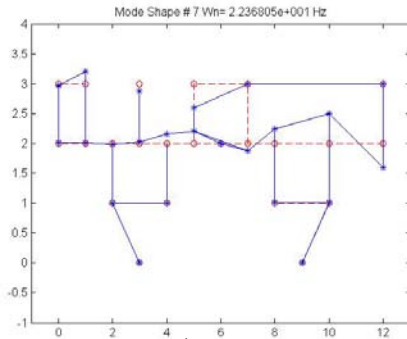


Figure 12: Frame bending w/Cab out of phase

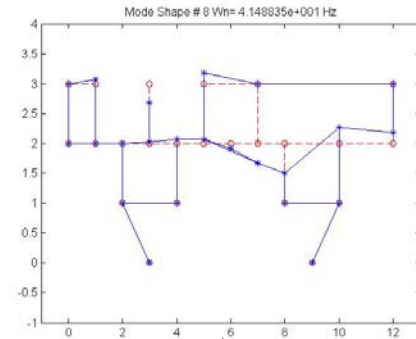


Figure 13: Frame bending w/powertrain bounce

bounce corresponds to the eighth natural frequency. The data has very little crew compartment excitation in the 4-8 Hz range which is the sensitive range for human occupants. In fact, the system has a significant amount of vibration in the 0-25 Hz range which corresponds to the ride quality and within the first 10 modes limited output within the 25-20,000 Hz range which corresponds to noise [9].

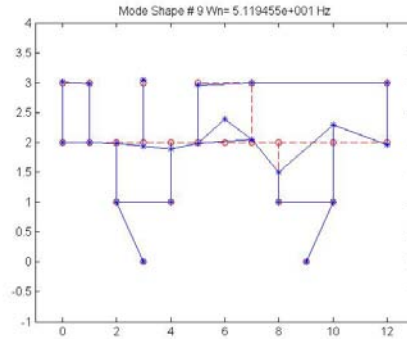


Figure 14: Frame Bending

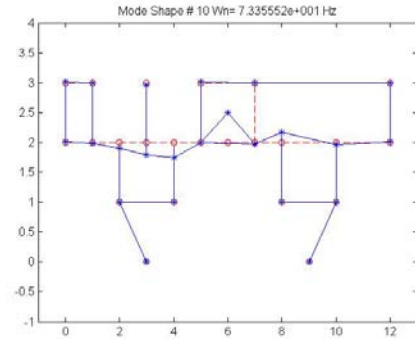


Figure 15: Frame Bending

3.1.2. Powertrain Excitation

The powertrain excitation is defined by equations 22-25 and is displayed in Figure 16. The peak of the excitation is centered at 45 Hz and filtered to zero less than 40 Hz and greater than 50 Hz. The spectrum corresponds to the idle rate of 900 RPM. Transfer Path Analysis (TPA) was used to map the powertrain input to the steering column identified in the first crew compartment element and the seat output identified as the second crew compartment element. Figure 17 displays the acceleration of the steering column with the input of the powertrain. Figure 18 displays the acceleration of the

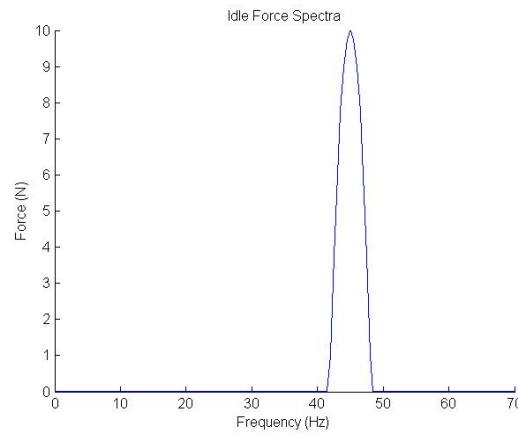


Figure 16: Idle

Force Spectra

seating element with the input parameter of the powertrain. The steering column idle input at 45 Hz is in the noise spectrum and a significant vibration impact onto the structure and audible noise. The seat excitation has the same shape and form as the steering column excitation given that the crew compartment weights are the same.

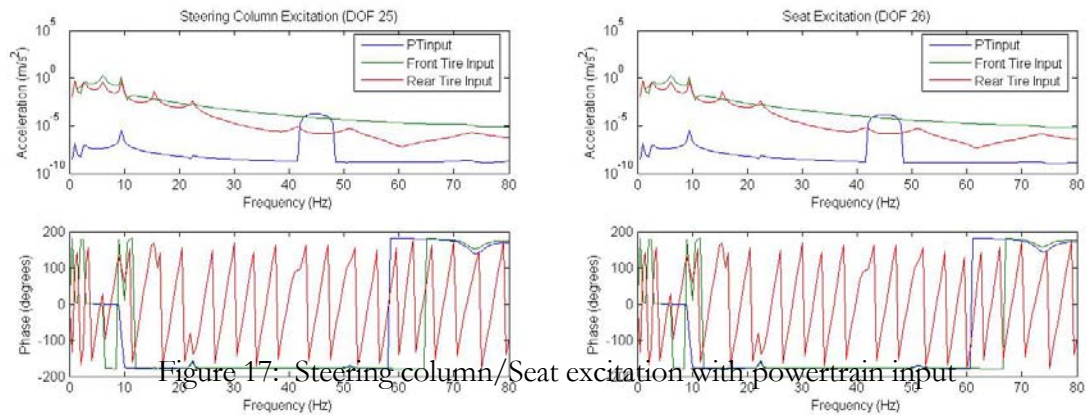


Figure 17: Steering column/Seat excitation with powertrain input

Note that both of the Figures indicate an anti-resonance at 2 Hz for both the powertrain and the front tire input. The HEMTT vehicle has the primary weight located at the front and middle of the axle without a load placed in the second and third bed element. The maximum vehicle weight is 100,000 pounds and with cargo capacity of 64,000 lbs. Figure 18 displays the seat and steering column excitation of the system at the maximum load.

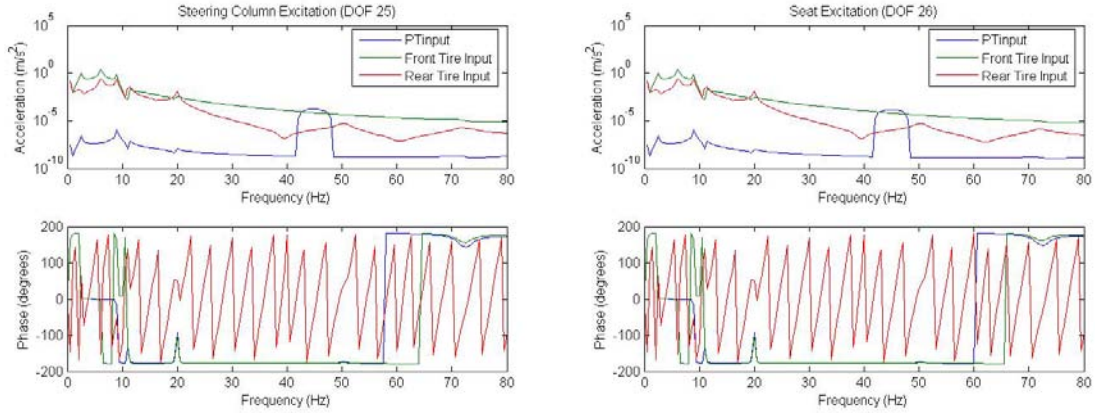


Figure 18: Steering column/Seat excitation with powertrain input at maximum load

3.1.3. Road Excitation

The road input for the front and rear suspension is illustrated in Figure 19 using equations 32 through 37. Note that the main difference is the phase delay associated

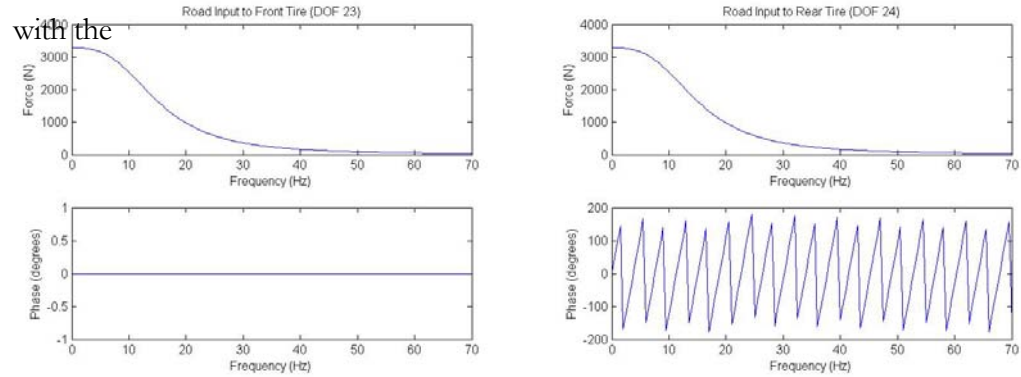


Figure 19: Front and Rear tire input

rear tire input which corresponds to the wheel base of the system. Figures 17 and 18 above display the front and rear tire input to the steering column and seat. Figure 20 displays the FRF for the steering column and seat in the unloaded condition.

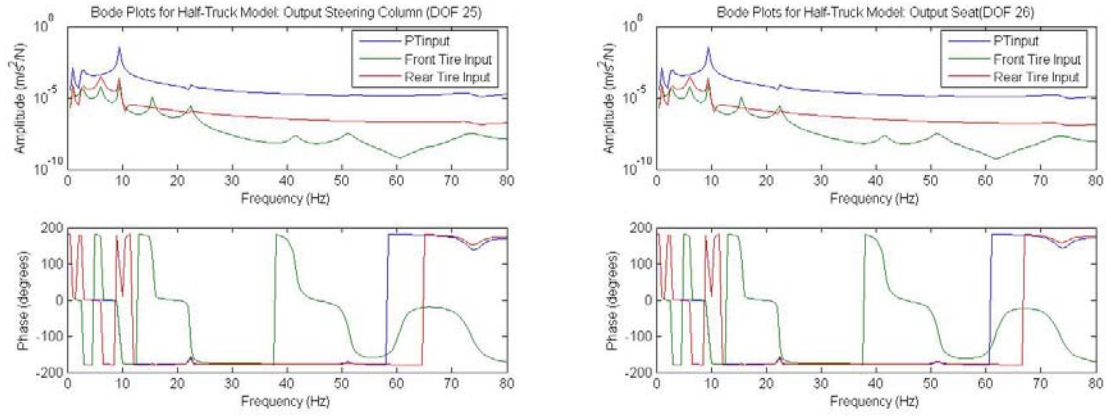


Figure 20: Steering column/Seat Frequency Response Function

3.1.4. Sensitivity Analysis

The sensitivity analysis was completed by addressing two distinct cases. The first case was to maximize the stiffness and mass variables by the identified increased based on assumptions and error approximations. The stiffness of the tires was increased by 20%, the stiffness of connecting the lumped masses to the frame was 15% and the stiffness of between elements was identified by 0.5%. All mass variables had 5% error identified. The second case was to maximize the stiffness variables and minimize the mass variables. The second case should provide higher natural frequencies given that the undamped natural frequency is

$$\omega_n = \sqrt{\frac{k}{m}} \quad [38]$$

where

k is the stiffness matrix; and

m is the mass matrix

The mode shapes for case 1 and case of the 10 PSF solution exhibit the same trends as the 10 PSF nominal solutions. Table 7 lists the natural frequencies for the 10 PSF case 1 solution and case 2 solutions. The natural frequency listed for the tenth mode is significantly different than the nominal value and the mode shapes for these frequencies are listed in Figure 21.

Table 7: Sensitivity Analysis of 10 PSF solution

	10 PSF Case 1	10PSF	10 PSF Case 2
ω_1	1.0093	0.966	1.0611
ω_2	2.6738	2.713	2.808
ω_3	6.5624	6.1499	6.8991
ω_4	6.5874	6.1709	6.9254
ω_5	9.4363	9.5018	9.8954
ω_6	15.295	15.556	16.08
ω_7	21.895	22.368	23.018
ω_8	40.593	41.488	42.676
ω_9	50.09	51.195	52.66
ω_{10}	72.388	73.356	76.1

The tenth mode shape for the nominal, case 1, and case 2 exhibit the same vehicle bending characteristics with the main distinction being the higher natural frequencies required to excite the system response. This is expected since case 2 focuses on

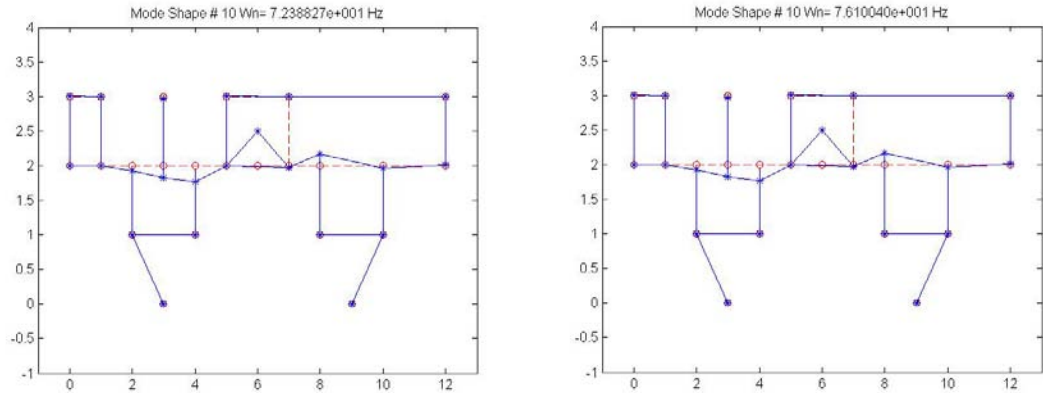


Figure 21: 10th Mode Shape excitation for case 1 and case 2 respectively

increasing the stiffness of the system which as equation 38 notes the trend as stiffness increases, an increase in the natural frequency is observed. The roughness of the frame bending is attributed to the node spacing, shorter separations between the nodes will prove smoother shaping of the frame bending. The higher natural frequency excited is located within the noise region of the frequency spectrum. The masses attached to the system display little movement.

3.2. 20 PSF Solution

3.2.1. Mode Shapes

The 20 PSF solution applies 492.8 kilograms of additional weight onto the front frame of the vehicle system nodes 1 and 3. The additional weight has little effect on the mode frequencies. The 20 PSF has little effect on the frequencies of the system. Table 8 lists the frequencies for first ten mode shapes of the 10 PSF and 20 PSF solutions.

Table 8: Natural Frequencies for 10 PSF and 20 PSF Crew Compartment

	10 PSF Case 1	10PSF	10 PSF Case 2	20PSF
ω_1	1.0093	0.966	1.0611	0.94605
ω_2	2.6738	2.713	2.808	2.5075
ω_3	6.5624	6.1499	6.8991	6.1498
ω_4	6.5874	6.1709	6.9254	6.1699
ω_5	9.4363	9.5018	9.8954	9.1542
ω_6	15.295	15.556	16.08	15.556
ω_7	21.895	22.368	23.018	22.367
ω_8	40.593	41.488	42.676	41.488
ω_9	50.09	51.195	52.66	51.195
ω_{10}	72.388	73.356	76.1	73.356

3.2.2. Powertrain Excitation

The same powertrain excitation is applied for the 20 PSF solution as for the 10 PSF solution. The powertrain excitation is defined by equations 22-25 and is displayed in Figure 16. Figure 22 displays the acceleration of the steering column and seat with the input of the powertrain. Note that both of the Figures indicate an anti-resonance for the front tire input at 10 Hz. The HEMTT vehicle has the primary weight located at the front and middle of the axle and with the increase of the crew compartment weight an anti-resonance is noted.

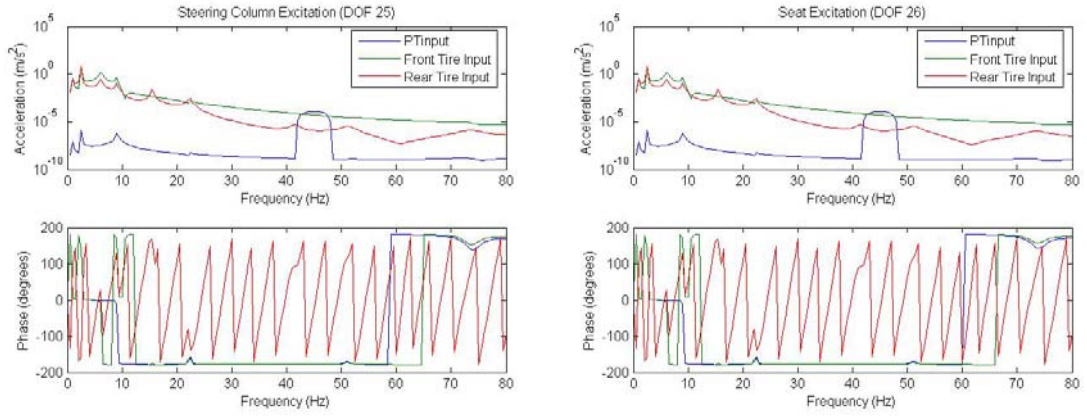


Figure 22: Steering column/Seat excitation with powertrain input at 20 PSF

3.2.3. Road Excitation

The same road excitation is applied for the 20 PSF solution as for the 10 PSF solution. The road input for the front and rear suspension is identified in Figure 19 using equations 32 through 37. Figure 23 displays the FRF for the steering column and seat in the unloaded condition.

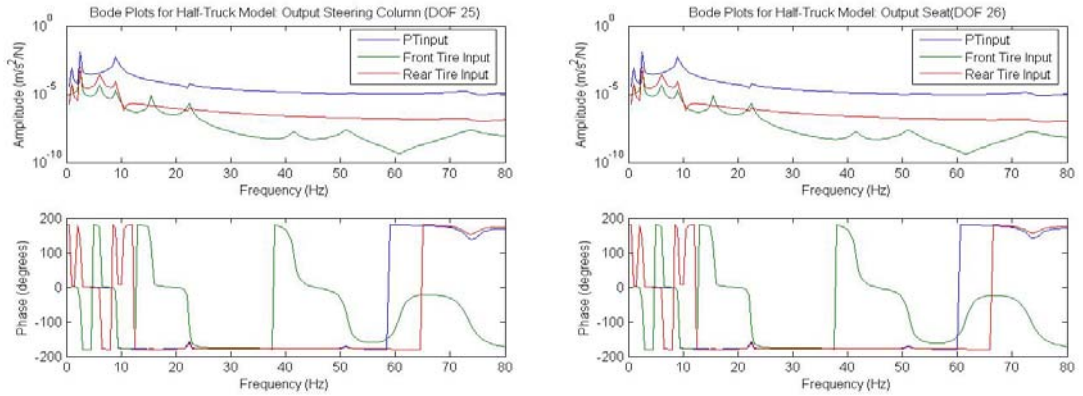


Figure 23: Steering column/Seat Frequency Response Function at 20 PSF

3.3. 30 PSF Solution

3.3.1. Mode Shapes

The 30 PSF solution applies 985.6 kilograms of additional weight onto the front frame of the vehicle system nodes 1 and 3. The additional weight has little effect on the

mode frequencies. Table 9 lists the frequencies for first ten mode shapes of the 10 PSF, 20 PSF, and 30 PSF solutions. The mode shapes for the 30 PSF solutions were similar to the 10 PSF and 20 PSF solutions.

Table 9: Natural Frequencies the PSF Crew Compartment

	10 PSF Case 1	10PSF	10 PSF Case 2	20PSF	30PSF
ω_1	1.0093	0.966	1.0611	0.94605	0.9264
ω_2	2.6738	2.713	2.808	2.5075	2.3551
ω_3	6.5624	6.1499	6.8991	6.1498	6.1498
ω_4	6.5874	6.1709	6.9254	6.1699	6.1692
ω_5	9.4363	9.5018	9.8954	9.1542	8.9392
ω_6	15.295	15.556	16.08	15.556	15.556
ω_7	21.895	22.368	23.018	22.367	22.366
ω_8	40.593	41.488	42.676	41.488	41.488
ω_9	50.09	51.195	52.66	51.195	51.194
ω_{10}	72.388	73.356	76.1	73.356	73.355

3.3.2. Powertrain Excitation

The same powertrain excitation is applied for the 30 PSF solution as for the 10 PSF solution with the main distinction the increased weight located on the front axle. The powertrain excitation is defined by equations 22-25 and is displayed in Figure 16. Figure 24 displays the acceleration of the steering column and seat with the input of the powertrain. Note that both of the Figures indicate an anti-resonance for the front tire input at 10 Hz which is very similar to the 20 PSF solution. The acceleration peaks of the FRF correspond to the identified natural frequencies listed in Table 9.

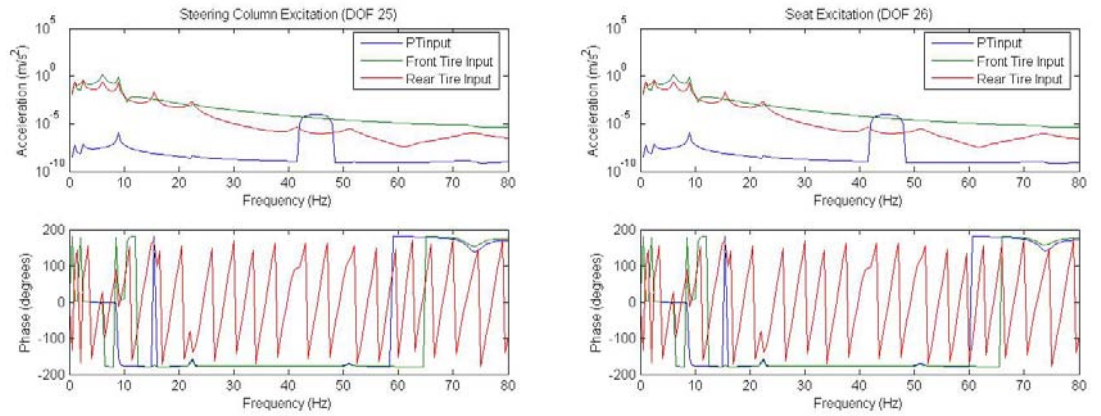


Figure 24: Steering column and seat acceleration with powertrain input at 30PSF

3.3.3. Road Excitation

The same road excitation is applied for the 30 PSF solution as for the 10 PSF solution. The road input for the front and rear suspension is identified in Figure 19 using equations 32 through 37. Figure 25 displays the FRF for the steering column and seat.

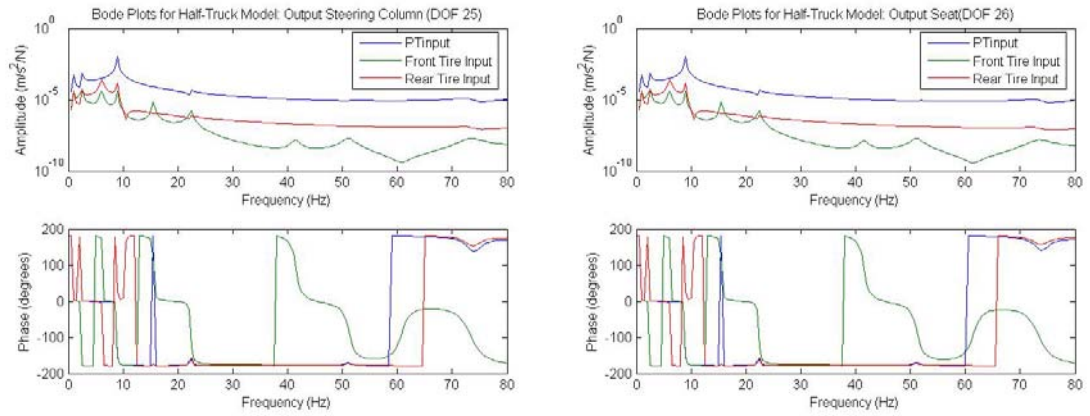


Figure 25: Steering column/Seat Frequency Response Function at 30 PSF

3.4. 40 PSF Solution

3.4.1. Mode Shapes

The 40 PSF solution applies 1,478.5 kilograms of additional weight onto the front frame of the vehicle system nodes 1 and 3. The additional weight has little effect on the mode frequencies. Table 9 lists the frequencies for first ten mode shapes of the 10 PSF, 20 PSF, 30 PSF, and 40 PSF solutions. The mode shapes for the 40 PSF solutions were similar to the crew compartment weights.

Table 9: Natural Frequencies for the Crew Compartment

	10 PSF Case 1	10PSF	10 PSF Case 2	20PSF	30PSF	40PSF
ω_1	1.0093	0.966	1.0611	0.94605	0.9264	0.90715
ω_2	2.6738	2.713	2.808	2.5075	2.3551	2.238
ω_3	6.5624	6.1499	6.8991	6.1498	6.1498	6.1498
ω_4	6.5874	6.1709	6.9254	6.1699	6.1692	6.1687
ω_5	9.4363	9.5018	9.8954	9.1542	8.9392	8.7936
ω_6	15.295	15.556	16.08	15.556	15.556	15.556
ω_7	21.895	22.368	23.018	22.367	22.366	22.366
ω_8	40.593	41.488	42.676	41.488	41.488	41.488
ω_9	50.09	51.195	52.66	51.195	51.194	51.194
ω_{10}	72.388	73.356	76.1	73.356	73.355	73.355

3.4.2. Powertrain Excitation

The same powertrain excitation is applied for the 40 PSF solution as for the 10 PSF solution with the main distinction the increased weight located on the front axle. The powertrain excitation is defined by equations 22-25 and is displayed in Figure 16. Figure 26 displays the acceleration of the steering column and seat with the input of the powertrain. Note that the anti-resonance located at the front tire continues to move to the left and is located just under 10 Hz.

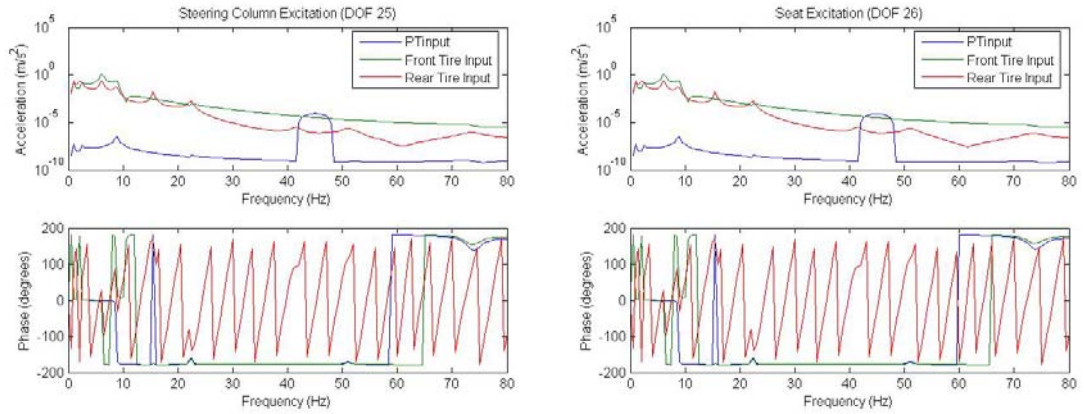


Figure 26: Steering column/seat acceleration with powertrain input at 40PSF

3.4.3. Road Excitation

The same road excitation is applied for the 40 PSF solution as for the 10 PSF solution. The road input for the front and rear suspension is identified in Figure 19 using equations 32 through 37. Figure 27 displays the FRF for the steering column and seat.

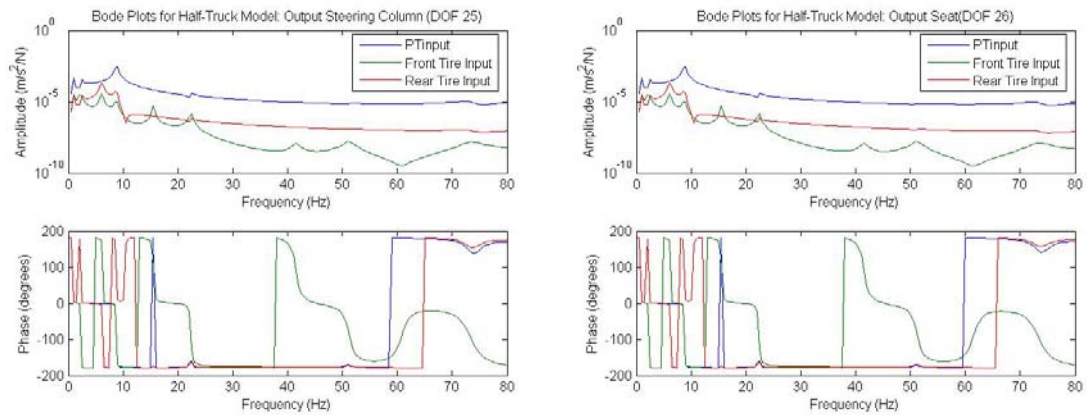


Figure 27: Steering column/Seat Frequency Response Function at 40 PSF

3.5. 50 PSF Solution

3.5.1. Mode Shapes

The 50 PSF solution applies 1,971.3 kilograms of additional weight onto the front frame of the vehicle system nodes 1 and 3. The additional weight has little effect on the mode frequencies. Table 10 lists the frequencies for first ten mode shapes of the 10 PSF, 20 PSF, 30 PSF, 40 PSF, and 50 PSF solutions. The mode shapes for the 50 PSF solutions were similar to the crew compartment weights.

Table 10: Natural Frequencies for the Crew Compartment

	10 PSF Case 1	10PSF	10 PSF Case 2	20PSF	30PSF	40PSF	50PSF
ω_1	1.0093	0.966	1.0611	0.94605	0.9264	0.90715	0.8884
ω_2	2.6738	2.713	2.808	2.5075	2.3551	2.238	2.1455
ω_3	6.5624	6.1499	6.8991	6.1498	6.1498	6.1498	6.1497
ω_4	6.5874	6.1709	6.9254	6.1699	6.1692	6.1687	6.1683
ω_5	9.4363	9.5018	9.8954	9.1542	8.9392	8.7936	8.6885
ω_6	15.295	15.556	16.08	15.556	15.556	15.556	15.556
ω_7	21.895	22.368	23.018	22.367	22.366	22.366	22.365
ω_8	40.593	41.488	42.676	41.488	41.488	41.488	41.488
ω_9	50.09	51.195	52.66	51.195	51.194	51.194	51.194
ω_{10}	72.388	73.356	76.1	73.356	73.355	73.355	73.355

3.5.2. Powertrain Excitation

The same powertrain excitation is applied for the 50 PSF solution as for the 10 PSF solution with the main distinction the increased weight located on the front axle. The powertrain excitation is defined by equations 22-25 and is displayed in Figure 16.

Figure 28 displays the acceleration of the steering column and seat with the input of the powertrain.

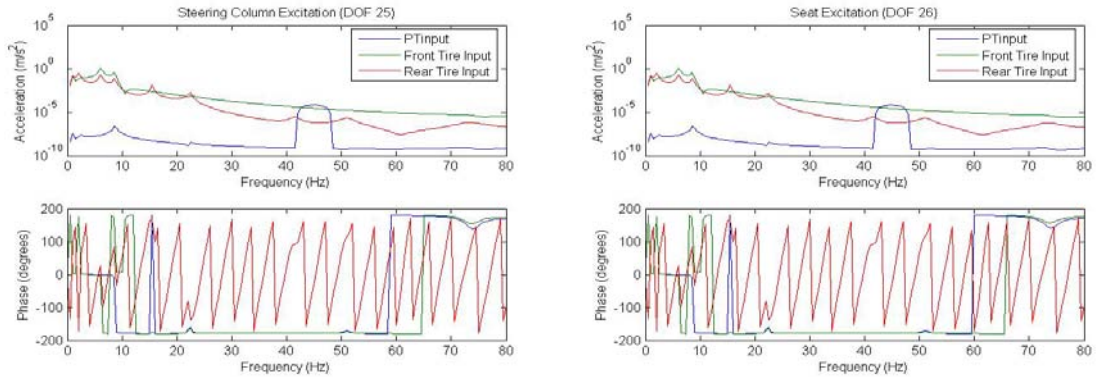


Figure 28: Steering column/seat acceleration with powertrain input at 50PSF

3.5.3. Road Excitation

The same road excitation is applied for the 50 PSF solution as for the 10 PSF solution. The road input for the front and rear suspension is identified in Figure 19 using equations 32 through 37. Figure 29 displays the FRF for the steering column and seat.

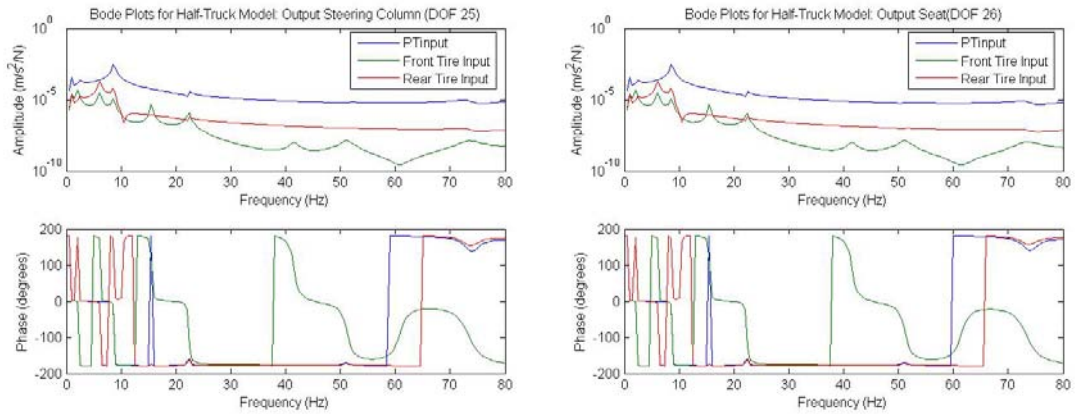


Figure 29: Steering column/Seat Frequency Response Function at 50 PSF

3.6. 60 PSF Solution

3.6.1. Mode Shapes

The 50 PSF solution applies 2,464.1 kilograms of additional weight onto the front frame of the vehicle system nodes 1 and 3. The additional weight has little effect on the mode frequencies. Table 11 lists the frequencies for first ten mode shapes of the all crew compartment weights. The results across all crew compartment weights indicate trends with the natural frequencies. The first mode, vehicle bounce,

Table 11: Natural Frequencies for crew compartment weights

	10 PSF Case 1	10PSF	10 PSF Case 2	20PSF	30PSF	40PSF	50PSF	60PSF
ω_1	1.0093	0.966	1.0611	0.94605	0.9264	0.90715	0.8884	0.8702
ω_2	2.6738	2.713	2.808	2.5075	2.3551	2.238	2.1455	2.0708
ω_3	6.5624	6.1499	6.8991	6.1498	6.1498	6.1498	6.1497	6.1497
ω_4	6.5874	6.1709	6.9254	6.1699	6.1692	6.1687	6.1683	6.168
ω_5	9.4363	9.5018	9.8954	9.1542	8.9392	8.7936	8.6885	8.6093
ω_6	15.295	15.556	16.08	15.556	15.556	15.556	15.556	15.556
ω_7	21.895	22.368	23.018	22.367	22.366	22.366	22.365	22.365
ω_8	40.593	41.488	42.676	41.488	41.488	41.488	41.488	41.488
ω_9	50.09	51.195	52.66	51.195	51.194	51.194	51.194	51.194
ω_{10}	72.388	73.356	76.1	73.356	73.355	73.355	73.355	73.355

occurs at a lower natural frequency as the weight is increased in the crew compartment location. The second mode shape which has several characteristics, vehicle pitch, crew compartment out of phase, engine bounce, and the bed out of phase bounce has a natural frequency decreases as the weight increases in the crew compartment. Modes three and four are relatively unchanged with the increased in weight. Mode shape three and four correspond to the front wheel hop out of phase. The fifth mode decreases as the weight increases since it incorporates crew compartment out of phase bounce, frame bending, and rear wheel hop. Mode shapes six, seven, eight, nine, and ten are relatively unaffected by the increased in weight of the crew compartment. Mode shape six corresponds to the frame bending. Mode seven and eight seem to have some crew compartment out-of-phase bounce, bed out-of-phase bounce and engine bounce along with frame bending. The ninth and tenth mode primarily corresponds to frame bending. Equation 38 validates the trends noted above, as the crew compartment weight increases for the frequencies that excite the crew compartment the overall natural frequency decreases for the undamped response since the equation is being divided by a higher number. An interesting observation is that the crew compartment weight at the 60 PSF solution is just slightly more than the powertrain components of the system.

3.6.2. Powertrain Excitation

The same powertrain excitation is applied for the 60 PSF solution as for the 10 PSF solution with the main distinction the increased weight located on the front axle. The powertrain excitation is defined by equations 22-25 and is displayed in Figure 16. Figure 30 displays the acceleration of the steering column and seat with the input of the powertrain. Figure 30 illustrates the powertrain excitation with at two of the lower frequencies, 0.87 Hz and 2.07 Hz, and another at 8.69 Hz besides the idle excitation centered at 45 Hz. The 7th mode centering around 22.36 Hz seems to have a slight powertrain excitation. However, the most significant natural frequency powertrain bounce is noted by the tallest peak at the 8.69 Hz. The excitation is noted by the peaks located in the FRF, the inverse parabolic shape corresponds to the idle excitation.

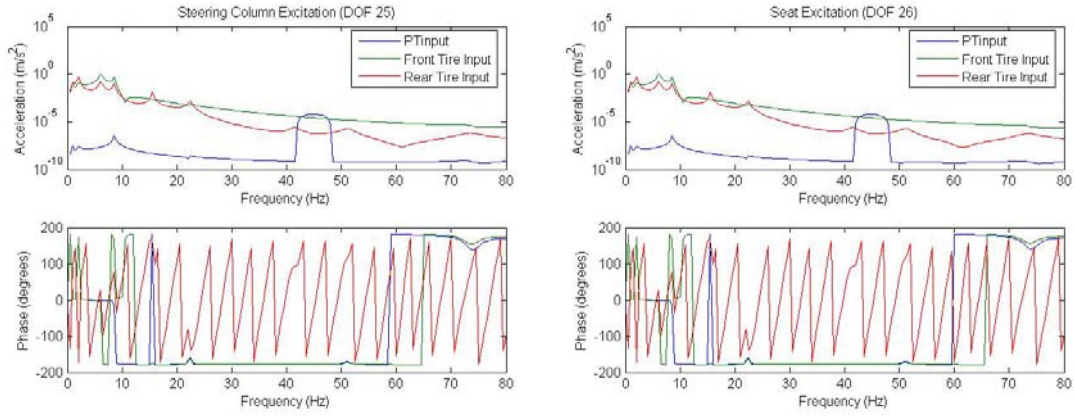


Figure 30: Steering column/seat acceleration with powertrain input at 60PSF

3.6.3. Road Excitation

The same road excitation is applied for the 60 PSF solution as for the 10 PSF solution. The road input for the front and rear suspense is identified in Figure 19 using equations 32 through 37. Figure 31 displays the FRF for the steering column and seat.

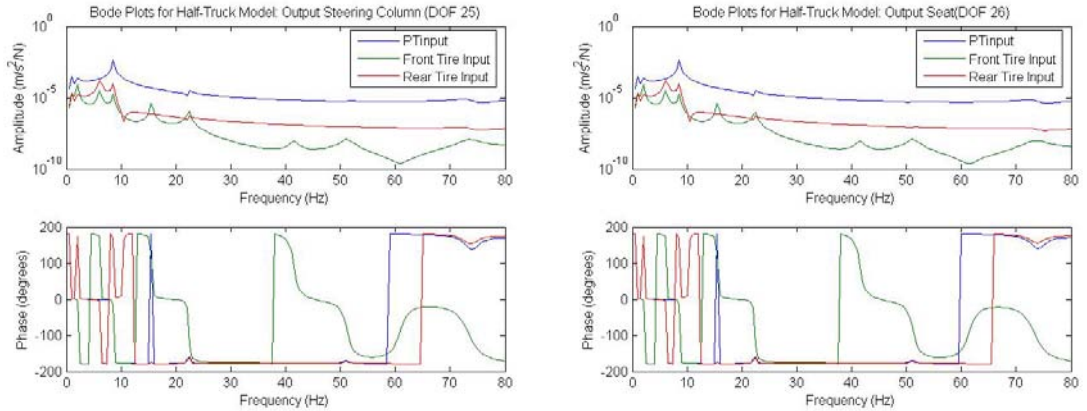


Figure 31: Steering column/Seat Frequency Response Function at 60 PSF

The steering column and seat excitation for the front tire input has a significant anti-resonance around 60 Hz. The FRF notes a significant amount of excitation with the seat and steering column with eight peaks visible. These peaks correspond to the natural frequencies of 0.87, 2.07, 6.17, 8.61, 15.56, 22.36, 41.49, and 51.19 Hz. The rear tire input primarily excites the first four natural frequencies listed as 0.87, 2.07,

6.17, and 8.61 Hz. The powertrain is excited slightly by the 0.87, 2.07, and 22.36 Hz natural frequencies with the predominate excitation located at the 8.61 Hz frequency.

3.6.4. Sensitivity Analysis

The sensitivity analysis was completed for the 60 PSF solution the same as for the 10 PSF solution using two distinct cases. The first case was to maximize the stiffness and mass variables by the identified increased based on assumptions and error approximations. The stiffness of the tires was increased by 20%, the stiffness of connecting the lumped masses to the frame was 15% and the stiffness of between elements was identified by 0.5%. All mass variables had 5% error identified. The second case was to maximize the stiffness variables and minimize the mass variables.

Table 12: Natural Frequencies for crew compartment weights

	10 PSF Case 1	10PSF	10 PSF Case 2	20PSF	30PSF	40PSF	50PSF	60 PSF Case 1	60PSF	60 PSF Case 2
ω_1	1.0093	0.966	1.0611	0.94605	0.9264	0.90715	0.8884	0.90868	0.8702	0.95523
ω_2	2.6738	2.713	2.808	2.5075	2.3551	2.238	2.1455	2.0419	2.0708	2.1438
ω_3	6.5624	6.1499	6.8991	6.1498	6.1498	6.1498	6.1497	6.5622	6.1497	6.8989
ω_4	6.5874	6.1709	6.9254	6.1699	6.1692	6.1687	6.1683	6.5841	6.168	6.9219
ω_5	9.4363	9.5018	9.8954	9.1542	8.9392	8.7936	8.6885	8.5513	8.6093	8.9691
ω_6	15.295	15.556	16.08	15.556	15.556	15.556	15.556	15.295	15.556	16.08
ω_7	21.895	22.368	23.018	22.367	22.366	22.366	22.365	21.892	22.365	23.015
ω_8	40.593	41.488	42.676	41.488	41.488	41.488	41.488	40.593	41.488	42.676
ω_9	50.09	51.195	52.66	51.195	51.194	51.194	51.194	50.09	51.194	52.66
ω_{10}	72.388	73.356	76.1	73.356	73.355	73.355	73.355	72.389	73.355	76.101

The sensitive analysis results are within the results of the previous crew compartment weights. An interesting observation is noted between case 2 of the 10 PSF solution and the 60 PSF solution. The natural frequencies for the sixth, seventh, eighth, ninth, and tenth mode shape are the same for both case. Where as with case 1, the similarities between the 10 PSF solution and the 60 PSF solution are for mode shapes three, four, six, seven eight, nine, and ten.

4. DISCUSSION

The parametric analysis of the HEMTT system varying the crew compartment weights from a 10 PSF solution to a 60 PSF showed very little impact to the overall mode shapes of the

vehicle system. The crew compartment weight will have a stronger influence on the vehicle dynamic properties and axle weight limitations than on the mode shapes of the system. Since the 10 PSF solution through the 60 PSF solution are similar, discussions will focus on the 60 PSF solution.

The system description identified two components of interest in the analysis, the first is the frame weight and stiffness and the second is the damping assumption. Since these two assumptions within the system description contribute to the response of the system, research will define why the assumptions were made and what if any impact they will have on the response. The system weight breakdown identifies the suspension systems, first element of the bed, and powertrain holding the primarily weight of the system. The frame supporting the system has a relatively low weight associated with it when comparing it to the above identified masses. Holen and Zellinger note that this is common for heavy vehicles since the primary purpose is to maximize payload so the frame is developed to be a relatively light structure that transmits forces efficiently with high frame stiffness [10]. The HEMTT is designed with a similar feature since its main mission is to transport payload. The frame is about a third of the weight of the powertrain and suspension system and the stiffness is identified to be 537 times as stiff as the powertrain connection to the frame and 56,531 times as stiff as the suspension system. The frame bending modes given the stiffness dominate the higher frequencies of the system.

The system damping was assumed to be defined using equation 2b. This is an assumption within the system that will have some impact on the overall mode shapes since the isolators play a critical role in noise and vibration. Researchers have shown that rubber isolators have amplitude and frequency dependence when subjected to harmonic displacements amplitudes in the 1-100 Hz frequency range [11] which is typical for highway transportation vehicles. Since the road input was not a harmonic displacement and damping of the tire was neglected based on the research of L.E. Kung since the intent of this paper was not to investigate the tire-patch interaction, but to represent the interaction in a simplified manner to study the road impact on crew compartment excitation; therefore, the modeling method was appropriate [12].

Noting the above resources and the intent of the paper to study the impact of crew compartment weight increase on the system's mode shapes, equation 2b effectively addressed the system damping and it is assumed to have minimal impact on the overall characterization of the crew compartment mode shapes. Further evidence that indicates that the system was modeled appropriately is from Lombaert and Degrande. Lombaert and Degrande indicate that the two eigenmodes that dominate the response of the vehicle are in the vertical plan: pitch and bounce modes at relatively low eigen frequencies between 0.8 and 3 Hz [13]. For the HEMTT analysis, the vehicle bounce corresponded to 0.8701 Hz and the vehicle pitch had a frequency at 2.07 Hz.

Given that the system and modeling approach used provides a first order model of the HEMTT system. The remainder of the discussion will focus on the crew compartment observations. The crew compartment was modeled as two separate mass elements connected by the stiffness associated with the thickness of the cab based on the pounds per square foot solution used to derive the thickness and weight of the system. The connection of the crew compartment to the frame was defined as the maximum weight of the crew compartment with a very small allowable displacement. Table 12 notes that the crew compartment weight has little effect on the natural frequency of the system, with the natural frequency response within ± 3 Hz of any result.

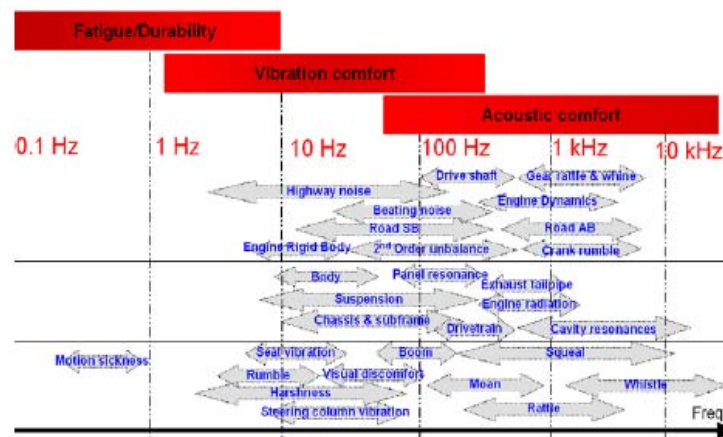


Figure 32: Noise, Vibration, and Harshness Sources in a vehicle [14]

The frequencies that had the most significant response for the crew compartment elements were at frequencies 0.87 Hz, 2.07 Hz, 8.61 Hz, 22.36 Hz, and 41.24 Hz corresponding to the 1st, 2nd, 5th, 7th, and 8th mode shape. Figure 32 denotes the typical noise, vibration, and harshness sources in a vehicle and the modes and frequencies map directly to those identified in the figure.

The first mode corresponds to the vehicle bounce and according to the figure is located within the fatigue/Durability region and may cause motion sickness when, for example, occupant seating fails to sufficiently provide isolation.. This motion coupled with the distortion experienced with looking through transparent armor will cause the soldier to exert significant amounts of energy and thus cause Soldier fatigue. Any driver's vision enhancement device or 360 degree situational vehicle device should be mounted to dampen this frequency from being transmitted to the console within the 0.1 Hz to 1 Hz range.

The second mode corresponds to the vehicle pitch and is located within the vibration comfort zone illustrated on Figure 32 and ride comfort as noted by Gillespie. The fifth mode corresponds to the frame bending with out-of-phase crew compartment and engine bounce excitation and is within seat vibration zone and engine rigid body zone. The seventh and eighth mode corresponds to frame bending with out-of-phase crew compartment and bed bounce with engine bounce and corresponds to the engine rigid body zone, body zone/chassis & sub-frame, and steering column vibration zone. Figure 31 confirms that the trends and behaviors identified for the HEMTT system fall within the typical NVH characteristics noted for the vehicle system.

The crew compartment excitations are critical for low frequencies and those that are within the human resonance frequency. Numerous researchers are investigating random vibration on the ride comfort of the occupants. The HEMTT system should be extensively studied with higher

fidelity models since it is used to re-supply combat vehicles and weapons systems within the area of operations and logs significant miles during any re-supply mission. Researchers have noted certain frequencies that impact the occupant in the vertical direction more than others. The frequencies from 3 to 7 Hz are areas where subjects are more sensitive to the vertical vibrations [15]. Additional occupant comfort issues are experienced in the vertical direction at two resonant frequencies, whole body resonance near 5 Hz and upper body resonance near 14 Hz [15]. The first order analysis of the HEMTT system has two natural frequencies that are within the noted intervals and a detailed FEA tool should be used to study the crew compartment and crew seating.

Soldiers are expected and required to multi-task while operating their tactical wheeled vehicle spanning from scouting the area to noting the instrument panel and commander's direction potentially causing Soldier fatigue. Protection requirements of the crew compartment have some impact on the Soldier given the vibration response from the system since all crew compartment solutions operated within the resonance zones identified to reduce ride comfort and cause fatigue. The resonances that have been noted for the characterization of the HEMTT system for the vehicle pitch are within the 3 to 7 Hz vertical sensitivity zone which needs to be addressed. Researchers have indicated that using seating systems to filter these vibrations are critical to occupant comfort and should be further researched for the HEMTT system. The HEMTT does not experience any other vibration within the critical areas.

It has been shown that the crew compartment weight for the HEMTT system has little impact on the natural frequencies of the system given the modeling assumptions used. Further analysis should focus on test methods for the crew compartment to measure the input forces to the crew compartment area associated with a normal duty cycle of the HEMTT system. Typical force excitations should include road inputs from standard Army proving grounds test, engine cooling fans/engine idle since those are dominant sources of noise and with the HEMTT are located directly behind the crew compartment in an attempt to validate the model.

5. CONCLUSION

A mathematical model for studying the effect of crew compartment growth was developed for a HEMTT vehicle system. The model completed a modal analysis of the half-truck model identifying the first ten natural frequencies and the systems mode shapes. The system was further enhanced to provide the response from a forced input of a road function and an idle condition of the identified system. The crew compartment weight increase was studied parametrically to assess the impact on the system's natural frequency. The computer model was not validated, but the results of the model with respect to the mode shapes are representational of researchers studying the same phenomena. The sensitivity analysis identified that the critical parameters of mass and stiffness provided the natural frequencies within $\pm 4\%$ of nominal cases.

This computer program enables one to assess the mode shapes of the HEMTT system given the lumped masses of crew compartment, unsprung front/rear mass, frame, powertrain, and bed of the system. The effect of varying the above properties can be studied to address the structural impact onto the overall HEMTT system with any changes to the mass and stiffness properties. To extend this computer model, it is necessary to validate the finding through additional experimentation to characterize the damping properties of the bushing connecting the lumped masses to the frame. Additional efforts should further address the crew compartment extensively to assess the impact of the rigid frame of the crew compartment with horizontal and bending associated to assess potential failures.

6. REFERENCES

- [1] Avitabile, Peter. “Experimental Modal Analysis (A Simple Non-Mathematical Presentation)”. Modal Analysis and Controls Laboratory. University of Massachusetts Lowell. Rev. 052700
- [2] Heo, J.H. and K.F. Ehmann. “A method for Sub structural Sensitive Synthesis.” Journal of Vibration and Acoustics. April 1991, Vol. 113 Pg 201-208.
- [3] DeClerck, J.P., AUTO599 Auto NVH, Winter 2007.
- [4] Marcus, M. and Minc, H. *Introduction to Linear Algebra*. New York: Dover, p. 145, 1988.
- [5] Juvinall, Robert, and Kurt M. Marshek. Fundamentals of Machine Component Design. New York: John Willey & Sons, 2000.
- [6] Beer, Ferdinand P., E. Russell Johnston, Jr., and John T. DeWolf. Mechanics of Materials. New York: McGraw-Hill, 2001.
- [7] Callister, William D. Jr. Materials Science and Engineering An Introduction. New York: John Willey & Sons, 2000.
- [8] Boresi, Arthur P., Richard J. Schmidt, and Omar M. Sidebottom. Advanced Mechanics of Materials. New York: John Willey & Sons, 1993.
- [9] Gillespie, Thomas. Fundamentals of Vehicle Dynamics. Warrendale: Society of Automotive Engineers, Inc., 1992.
- [10] Holen, Peter, and Mathias Zellinger. “Aspects on damper-attachment compliance.” International Journal of Vehicle Design, Vol. 40, No. 1,2,3; 2006.
- [11] Garcia, Maria-José. “Engineering rubber bushing stiffness formulas including dynamic amplitude dependence.” Licensed Thesis, Royal Institute of Technology, Stockholm; 2006.
- [12] Kung, L.E., W. Soedel, and T.Y. Yang. “On the vibration transmission of a rolling tire on a suspension system due to periodic tread excitation.” Journal of Sound and Vibration. Vol 115(1), Pg 37-63; 1987.
- [13] Lombaert, G. and G. Degrande. “The experimental validation of a numerical model for the prediction of the vibrations in the free field produced by road traffic.” Journal of Sound and Vibration. Vol 262, pgs 309-331; 2003.

- [14] Møller, Nis and Mehdi Batel. "Obtaining Maximum Value from Source/Path Contribution Analysis." Brüel & Kjaer Sound and Vibration Measurements A/S. DK 2850, Naerum, Denmark.
- [15] Demić, M., J. Lukić, and Ž. Milić. "Some Aspects of the Investigation of Random Vibration Influence on Ride Comfort." Journal of Sound and Vibration. Vol. 253(1) Pgs. 109-129; 2002.

Appendix A

```

clear
close all

%NVH Capstone Project: Half-Truck Model of a Heavy Duty Off-Road
Vehicle
%XM1120A4
%Heather Molitoris
%Fall 2007

%Global Variables
%Frame
L=10.4648; %units are in meters
rhoa=40.002*2; %units are in kg/m
EI=750080.587164*2; %Units are in N-m*m
e=10; %number of elements
l=[1.31064 0.59436 0.762 0.762 0.59436 1.07188 1.07188 1.07188 1.524
1.7018];
L_check=l(1)+l(2)+l(3)+l(4)+l(5)+l(6)+l(7)+l(8)+l(9)+l(10);

%powertrain
kpm=243453.6*100; %units are in N/m

%Suspension
%kwb1=kwb2
kwb1=115.6*1000; %units are in N/m
kwb2=115.6*1000; %units are in N/m
%kt1=kt2=kt3=kt4
kt1=1641*1000; %units are in N/m
kt2=1641*1000; %units are in N/m
kt3=1641*1000; %units are in N/m
kt4=1641*1000; %units are in N/m

%Truck Cab
kc=[1291000 2582000 3854000 5145000 6435000 7726000]*1000; %units are
in N/m
    %10PSF    20PSF    30PSF    40PSF    50PSF    60PSF
kcm=917500*100; %units are in N/m

%Truck Bed
kb=41433.257951*1000; %units are in N/m
kbm=7597206.42763*100; %units are in N/m

%*****Stiffness Matrix for Frame
k1=EI*[12/l(1)^3    6/l(1)^2 -12/l(1)^3 6/l(1)^2;
        6/l(1)^2    4/l(1) -6/l(1)^2 2/l(1);
       -12/l(1)^3  -6/l(1)^2 12/l(1)^3 -6/l(1)^2;
        6/l(1)^2    2/l(1) -6/l(1)^2 4/l(1)];

k2=EI*[12/l(2)^3    6/l(2)^2 -12/l(2)^3 6/l(2)^2;
        6/l(2)^2    4/l(2) -6/l(2)^2 2/l(2);
       -12/l(2)^3  -6/l(2)^2 12/l(2)^3 -6/l(2)^2;
        6/l(2)^2    2/l(2) -6/l(2)^2 4/l(2)];

k3=EI*[12/l(3)^3    6/l(3)^2 -12/l(3)^3 6/l(3)^2;

```

```

        6/1(3)^2    4/1(3) -6/1(3)^2    2/1(3);
        -12/1(3)^3 -6/1(3)^2 12/1(3)^3 -6/1(3)^2;
        6/1(3)^2    2/1(3)   -6/1(3)^2 4/1(3)];

k4=EI*[12/1(4)^3    6/1(4)^2 -12/1(4)^3 6/1(4)^2;
        6/1(4)^2    4/1(4) -6/1(4)^2    2/1(4);
        -12/1(4)^3 -6/1(4)^2 12/1(4)^3 -6/1(4)^2;
        6/1(4)^2    2/1(4)   -6/1(4)^2 4/1(4)];

k5=EI*[12/1(5)^3    6/1(5)^2 -12/1(5)^3 6/1(5)^2;
        6/1(5)^2    4/1(5) -6/1(5)^2    2/1(5);
        -12/1(5)^3 -6/1(5)^2 12/1(5)^3 -6/1(5)^2;
        6/1(5)^2    2/1(5)   -6/1(5)^2 4/1(5)];

k6=EI*[12/1(6)^3    6/1(6)^2 -12/1(6)^3 6/1(6)^2;
        6/1(6)^2    4/1(6) -6/1(6)^2    2/1(6);
        -12/1(6)^3 -6/1(6)^2 12/1(6)^3 -6/1(6)^2;
        6/1(6)^2    2/1(6)   -6/1(6)^2 4/1(6)];

k7=EI*[12/1(7)^3    6/1(7)^2 -12/1(7)^3 6/1(7)^2;
        6/1(7)^2    4/1(7) -6/1(7)^2    2/1(7);
        -12/1(7)^3 -6/1(7)^2 12/1(7)^3 -6/1(7)^2;
        6/1(7)^2    2/1(7)   -6/1(7)^2 4/1(7)];

k8=EI*[12/1(8)^3    6/1(8)^2 -12/1(8)^3 6/1(8)^2;
        6/1(8)^2    4/1(8) -6/1(8)^2    2/1(8);
        -12/1(8)^3 -6/1(8)^2 12/1(8)^3 -6/1(8)^2;
        6/1(8)^2    2/1(8)   -6/1(8)^2 4/1(8)];

k9=EI*[12/1(9)^3    6/1(9)^2 -12/1(9)^3 6/1(9)^2;
        6/1(9)^2    4/1(9) -6/1(9)^2    2/1(9);
        -12/1(9)^3 -6/1(9)^2 12/1(9)^3 -6/1(9)^2;
        6/1(9)^2    2/1(9)   -6/1(9)^2 4/1(9)];

k10=EI*[12/1(10)^3    6/1(10)^2 -12/1(10)^3 6/1(10)^2;
        6/1(10)^2    4/1(10) -6/1(10)^2    2/1(10);
        -12/1(10)^3 -6/1(10)^2 12/1(10)^3 -6/1(10)^2;
        6/1(10)^2    2/1(10)   -6/1(10)^2 4/1(10)];

%*****Mass Matrix for Frame
m1=(rhoa/420)*[156*1(1) 22*1(1)^2 54*1(1)    -13*1(1)^2;
               22*1(1)^2 4*1(1)^3   13*1(1)^2 -3*1(1)^3;
               54*1(1)   13*1(1)^2 156*1(1)   -22*1(1)^2;
               -13*1(1)^2 -3*1(1)^3 -22*1(1)^2 4*1(1)^3];

m2=(rhoa/420)*[156*1(2) 22*1(2)^2 54*1(2)    -13*1(2)^2;
               22*1(2)^2 4*1(2)^3   13*1(2)^2 -3*1(2)^3;
               54*1(2)   13*1(2)^2 156*1(2)   -22*1(2)^2;
               -13*1(2)^2 -3*1(2)^3 -22*1(2)^2 4*1(2)^3];

m3=(rhoa/420)*[156*1(3) 22*1(3)^2 54*1(3)    -13*1(3)^2;
               22*1(3)^2 4*1(3)^3   13*1(3)^2 -3*1(3)^3;
               54*1(3)   13*1(3)^2 156*1(3)   -22*1(3)^2;
               -13*1(3)^2 -3*1(3)^3 -22*1(3)^2 4*1(3)^3];

```

```

m4=(rhoa/420)*[156*1(4) 22*1(4)^2 54*1(4) -13*1(4)^2;
                22*1(4)^2 4*1(4)^3 13*1(4)^2 -3*1(4)^3;
                54*1(4) 13*1(4)^2 156*1(4) -22*1(4)^2;
                -13*1(4)^2 -3*1(4)^3 -22*1(4)^2 4*1(4)^3];

m5=(rhoa/420)*[156*1(5) 22*1(5)^2 54*1(5) -13*1(5)^2;
                22*1(5)^2 4*1(5)^3 13*1(5)^2 -3*1(5)^3;
                54*1(5) 13*1(5)^2 156*1(5) -22*1(5)^2;
                -13*1(5)^2 -3*1(5)^3 -22*1(5)^2 4*1(5)^3];

m6=(rhoa/420)*[156*1(6) 22*1(6)^2 54*1(6) -13*1(6)^2;
                22*1(6)^2 4*1(6)^3 13*1(6)^2 -3*1(6)^3;
                54*1(6) 13*1(6)^2 156*1(6) -22*1(6)^2;
                -13*1(6)^2 -3*1(6)^3 -22*1(6)^2 4*1(6)^3];

m7=(rhoa/420)*[156*1(7) 22*1(7)^2 54*1(7) -13*1(7)^2;
                22*1(7)^2 4*1(7)^3 13*1(7)^2 -3*1(7)^3;
                54*1(7) 13*1(7)^2 156*1(7) -22*1(7)^2;
                -13*1(7)^2 -3*1(7)^3 -22*1(7)^2 4*1(7)^3];

m8=(rhoa/420)*[156*1(8) 22*1(8)^2 54*1(8) -13*1(8)^2;
                22*1(8)^2 4*1(8)^3 13*1(8)^2 -3*1(8)^3;
                54*1(8) 13*1(8)^2 156*1(8) -22*1(8)^2;
                -13*1(8)^2 -3*1(8)^3 -22*1(8)^2 4*1(8)^3];

m9=(rhoa/420)*[156*1(9) 22*1(9)^2 54*1(9) -13*1(9)^2;
                22*1(9)^2 4*1(9)^3 13*1(9)^2 -3*1(9)^3;
                54*1(9) 13*1(9)^2 156*1(9) -22*1(9)^2;
                -13*1(9)^2 -3*1(9)^3 -22*1(9)^2 4*1(9)^3];

m10=(rhoa/420)*[156*1(10) 22*1(10)^2 54*1(10) -13*1(10)^2;
                 22*1(10)^2 4*1(10)^3 13*1(10)^2 -3*1(10)^3;
                 54*1(10) 13*1(10)^2 156*1(10) -22*1(10)^2;
                 -13*1(10)^2 -3*1(10)^3 -22*1(10)^2 4*1(10)^3];

%Transformation Matrices for the 22 DOF Frame
T1=[1 0 0 0 0 0 0 0 0 0 0 0 0 0 0 0 0 0 0 0 0 0;
    0 1 0 0 0 0 0 0 0 0 0 0 0 0 0 0 0 0 0 0 0 0;
    0 0 1 0 0 0 0 0 0 0 0 0 0 0 0 0 0 0 0 0 0 0;
    0 0 0 1 0 0 0 0 0 0 0 0 0 0 0 0 0 0 0 0 0 0];

T2=[0 0 1 0 0 0 0 0 0 0 0 0 0 0 0 0 0 0 0 0 0 0;
    0 0 0 1 0 0 0 0 0 0 0 0 0 0 0 0 0 0 0 0 0 0;
    0 0 0 0 1 0 0 0 0 0 0 0 0 0 0 0 0 0 0 0 0 0;
    0 0 0 0 0 1 0 0 0 0 0 0 0 0 0 0 0 0 0 0 0 0];

T3=[0 0 0 0 1 0 0 0 0 0 0 0 0 0 0 0 0 0 0 0 0 0;
    0 0 0 0 0 1 0 0 0 0 0 0 0 0 0 0 0 0 0 0 0 0;
    0 0 0 0 0 0 1 0 0 0 0 0 0 0 0 0 0 0 0 0 0 0;
    0 0 0 0 0 0 0 1 0 0 0 0 0 0 0 0 0 0 0 0 0 0];

T4=[0 0 0 0 0 0 1 0 0 0 0 0 0 0 0 0 0 0 0 0 0 0;
    0 0 0 0 0 0 0 1 0 0 0 0 0 0 0 0 0 0 0 0 0 0];

```

```

0 0 0 0 0 0 0 0 0 0 1 0 0 0 0 0 0 0 0 0 0 0 0 0;
0 0 0 0 0 0 0 0 0 0 0 1 0 0 0 0 0 0 0 0 0 0 0 0];

T5=[0 0 0 0 0 0 0 0 0 0 1 0 0 0 0 0 0 0 0 0 0 0 0 0;
0 0 0 0 0 0 0 0 0 0 0 1 0 0 0 0 0 0 0 0 0 0 0 0;
0 0 0 0 0 0 0 0 0 0 0 0 1 0 0 0 0 0 0 0 0 0 0 0;
0 0 0 0 0 0 0 0 0 0 0 0 0 1 0 0 0 0 0 0 0 0 0 0];

T6=[0 0 0 0 0 0 0 0 0 0 0 0 1 0 0 0 0 0 0 0 0 0 0 0;
0 0 0 0 0 0 0 0 0 0 0 0 0 1 0 0 0 0 0 0 0 0 0 0;
0 0 0 0 0 0 0 0 0 0 0 0 0 0 1 0 0 0 0 0 0 0 0 0;
0 0 0 0 0 0 0 0 0 0 0 0 0 0 0 1 0 0 0 0 0 0 0 0];

T7=[0 0 0 0 0 0 0 0 0 0 0 0 0 0 0 1 0 0 0 0 0 0 0 0;
0 0 0 0 0 0 0 0 0 0 0 0 0 0 0 0 1 0 0 0 0 0 0 0;
0 0 0 0 0 0 0 0 0 0 0 0 0 0 0 0 0 1 0 0 0 0 0 0;
0 0 0 0 0 0 0 0 0 0 0 0 0 0 0 0 0 0 1 0 0 0 0 0];

T8=[0 0 0 0 0 0 0 0 0 0 0 0 0 0 0 0 0 1 0 0 0 0 0 0;
0 0 0 0 0 0 0 0 0 0 0 0 0 0 0 0 0 0 1 0 0 0 0 0;
0 0 0 0 0 0 0 0 0 0 0 0 0 0 0 0 0 0 0 1 0 0 0 0;
0 0 0 0 0 0 0 0 0 0 0 0 0 0 0 0 0 0 0 0 1 0 0 0];

T9=[0 0 0 0 0 0 0 0 0 0 0 0 0 0 0 0 0 0 0 1 0 0 0 0;
0 0 0 0 0 0 0 0 0 0 0 0 0 0 0 0 0 0 0 0 1 0 0 0;
0 0 0 0 0 0 0 0 0 0 0 0 0 0 0 0 0 0 0 0 0 1 0 0;
0 0 0 0 0 0 0 0 0 0 0 0 0 0 0 0 0 0 0 0 0 0 1 0];

T10=[0 0 0 0 0 0 0 0 0 0 0 0 0 0 0 0 0 0 0 0 0 1 0 0;
0 0 0 0 0 0 0 0 0 0 0 0 0 0 0 0 0 0 0 0 0 0 1 0;
0 0 0 0 0 0 0 0 0 0 0 0 0 0 0 0 0 0 0 0 0 0 0 1;
0 0 0 0 0 0 0 0 0 0 0 0 0 0 0 0 0 0 0 0 0 0 0 1];

%Mass Calculations for Frame
M1=T1'*m1*T1;
M2=T2'*m2*T2;
M3=T3'*m3*T3;
M4=T4'*m4*T4;
M5=T5'*m5*T5;
M6=T6'*m6*T6;
M7=T7'*m7*T7;
M8=T8'*m8*T8;
M9=T9'*m9*T9;
M10=T10'*m10*T10;

M_Frame=M1+M2+M3+M4+M5+M6+M7+M8+M9+M10;

%Spring Calculations for Frame
K1=T1'*k1*T1;
K2=T2'*k2*T2;
K3=T3'*k3*T3;
K4=T4'*k4*T4;
K5=T5'*k5*T5;
K6=T6'*k6*T6;

```

```

K7=T7'*k7*T7;
K8=T8'*k8*T8;
K9=T9'*k9*T9;
K10=T10'*k10*T10;

K_Frame=K1+K2+K3+K4+K5+K6+K7+K8+K9+K10;

k8by22=[0 0 0 0 0 0 0 0;
         0 0 0 0 0 0 0 0;
         0 0 0 0 0 0 0 0;
         0 0 0 0 0 0 0 0;
         0 0 0 0 0 0 0 0;
         0 0 0 0 0 0 0 0;
         0 0 0 0 0 0 0 0;
         0 0 0 0 0 0 0 0;
         0 0 0 0 0 0 0 0;
         0 0 0 0 0 0 0 0;
         0 0 0 0 0 0 0 0;
         0 0 0 0 0 0 0 0;
         0 0 0 0 0 0 0 0;
         0 0 0 0 0 0 0 0;
         0 0 0 0 0 0 0 0;
         0 0 0 0 0 0 0 0;
         0 0 0 0 0 0 0 0;
         0 0 0 0 0 0 0 0;
         0 0 0 0 0 0 0 0;
         0 0 0 0 0 0 0 0;
         0 0 0 0 0 0 0 0];

k_hor30=horzcat(K_Frame, k8by22);

k30by8=[0 0 0 0 0 0 0 0 0 0 0 0 0 0 0 0 0 0 0 0 0 0 0 0 0 0 0 0;
         0 0 0 0 0 0 0 0 0 0 0 0 0 0 0 0 0 0 0 0 0 0 0 0 0 0 0 0;
         0 0 0 0 0 0 0 0 0 0 0 0 0 0 0 0 0 0 0 0 0 0 0 0 0 0 0 0;
         0 0 0 0 0 0 0 0 0 0 0 0 0 0 0 0 0 0 0 0 0 0 0 0 0 0 0 0;
         0 0 0 0 0 0 0 0 0 0 0 0 0 0 0 0 0 0 0 0 0 0 0 0 0 0 0 0;
         0 0 0 0 0 0 0 0 0 0 0 0 0 0 0 0 0 0 0 0 0 0 0 0 0 0 0 0;
         0 0 0 0 0 0 0 0 0 0 0 0 0 0 0 0 0 0 0 0 0 0 0 0 0 0 0 0;
         0 0 0 0 0 0 0 0 0 0 0 0 0 0 0 0 0 0 0 0 0 0 0 0 0 0 0 0];

k_ver30=vertcat(k_hor30, k30by8);

%*****END OF FEA For Frame

%*****EOM Mass Matrix Development
%m_eom_10=[2339.811 2339.811 700.006 700.006 2308.785 3749.301
14514.956 14514.954];
    %loaded bed      %mf      mr      mc1      mc2      mpt      mb1
mb2      mb3      Units are in Kg

```

```
m_eom_10=[2339.811 2339.811 700.006 700.006 2308.785 3609.764 1524.123
1524.123];
```

```
      %mf      mr      mc1      mc2      mpt      mb1      mb2
mb3      Units are in Kg
```

```
m_eom_20=[2339.811 2339.811 946.420 946.420 2308.785 3609.764 1524.123
1524.123];
```

```
      %mf      mr      mc1      mc2      mpt      mb1      mb2
mb3      Units are in Kg
```

```
m_eom_30=[2339.811 2339.811 1192.835 1192.835 2308.785 3609.764
1524.123 1524.123];
```

```
      %mf      mr      mc1      mc2      mpt      mb1      mb2
mb3      Units are in Kg
```

```
m_eom_40=[2339.811 2339.811 1439.249 1439.249 2308.785 3609.764
1524.123 1524.123];
```

```
      %mf      mr      mc1      mc2      mpt      mb1      mb2
mb3      Units are in Kg
```

```
m_eom_50=[2339.811 2339.811 1685.663 1685.663 2308.785 3609.764
1524.123 1524.123];
```

```
      %mf      mr      mc1      mc2      mpt      mb1      mb2
mb3      Units are in Kg
```

```
m_eom_60=[2339.811 2339.811 1932.077 1932.077 2308.785 3609.764
1524.123 1524.123];
```

```
      %mf      mr      mc1      mc2      mpt      mb1      mb2
mb3      Units are in Kg
```

```
M_EOM_10=[m_eom_10(1) 0      0      0      0      0      0      0;
0      m_eom_10(2) 0      0      0      0      0      0;
0      0      m_eom_10(3) 0      0      0      0      0;
0      0      0      m_eom_10(4) 0      0      0      0;
0      0      0      0      m_eom_10(5) 0      0      0;
0      0      0      0      0      m_eom_10(6) 0      0;
0      0      0      0      0      0      m_eom_10(7) 0;
0      0      0      0      0      0      0      m_eom_10(8)];
```

```
M_EOM_20=[m_eom_20(1) 0      0      0      0      0      0      0;
0      m_eom_20(2) 0      0      0      0      0      0;
0      0      m_eom_20(3) 0      0      0      0      0;
0      0      0      m_eom_20(4) 0      0      0      0;
0      0      0      0      m_eom_20(5) 0      0      0;
0      0      0      0      0      m_eom_20(6) 0      0;
0      0      0      0      0      0      m_eom_20(7) 0;
0      0      0      0      0      0      0      m_eom_20(8)];
```

```
M_EOM_30=[m_eom_30(1) 0      0      0      0      0      0      0;
0      m_eom_30(2) 0      0      0      0      0      0;
0      0      m_eom_30(3) 0      0      0      0      0;
0      0      0      m_eom_30(4) 0      0      0      0;
0      0      0      0      m_eom_30(5) 0      0      0;
```

```

0      0      0      0      0      m_eom_30(6) 0      0;
0      0      0      0      0      0      m_eom_30(7) 0;
0      0      0      0      0      0      0      m_eom_30(8)];

M_EOM_40=[m_eom_40(1) 0      0      0      0      0      0      0;
0      m_eom_40(2) 0      0      0      0      0      0;
0      0      m_eom_40(3) 0      0      0      0      0;
0      0      0      m_eom_40(4) 0      0      0      0;
0      0      0      0      m_eom_40(5) 0      0      0;
0      0      0      0      0      m_eom_40(6) 0      0;
0      0      0      0      0      0      m_eom_40(7) 0;
0      0      0      0      0      0      0      m_eom_40(8)];

M_EOM_50=[m_eom_50(1) 0      0      0      0      0      0      0;
0      m_eom_50(2) 0      0      0      0      0      0;
0      0      m_eom_50(3) 0      0      0      0      0;
0      0      0      m_eom_50(4) 0      0      0      0;
0      0      0      0      m_eom_50(5) 0      0      0;
0      0      0      0      0      m_eom_50(6) 0      0;
0      0      0      0      0      0      m_eom_50(7) 0;
0      0      0      0      0      0      0      m_eom_50(8)];

M_EOM_60=[m_eom_60(1) 0      0      0      0      0      0      0;
0      m_eom_60(2) 0      0      0      0      0      0;
0      0      m_eom_60(3) 0      0      0      0      0;
0      0      0      m_eom_60(4) 0      0      0      0;
0      0      0      0      m_eom_60(5) 0      0      0;
0      0      0      0      0      m_eom_60(6) 0      0;
0      0      0      0      0      0      m_eom_60(7) 0;
0      0      0      0      0      0      0      m_eom_60(8)];

%EOM Spring Development
%NOTE TO SELF: Do not include the rotational components in element
mapping
%just the translation DOF.

%Connecting the lumped masses to the frame

%DOF 1 Connects to DOF 25
%1 2 3 4 5 6 7 8 9 10 11 12 13 14 15 16 17 18 19 20 21 22 23 24
25 26 27 28 29 30
T1_25=[1 0 0 0 0 0 0 0 0 0 0 0 0 0 0 0 0 0 0 0 0 0 0
0 0 0 0 0];
%0 0 0 0 0 0 0 0 0 0 0 0 0 0 0 0 0 0 0 0 0 0 1
0 0 0 0 0];
k1_25=[kcm -kcm;
-kcm kcm];
K1_25=T1_25'*k1_25*T1_25;

%DOF 3 connects to DOF 26
%1 2 3 4 5 6 7 8 9 10 11 12 13 14 15 16 17 18 19 20 21 22 23 24
25 26 27 28 29 30
T3_26=[0 0 1 0 0 0 0 0 0 0 0 0 0 0 0 0 0 0 0 0 0 0 0
0 0 0 0 0];

```

```

0 0 0 0 0 0 0 0 0 0 0 0 0 0 0 0 0 0 0 0 0 0 0 0 0 0
1 0 0 0 0 0];
k3_26=[kcm -kcm;
      -kcm kcm];
K3_26=T3_26'*k3_26*T3_26;

%DOF 5 Connects to DOF 23
%1 2 3 4 5 6 7 8 9 10 11 12 13 14 15 16 17 18 19 20 21 22 23 24
25 26 27 28 29 30
T5_23=[0 0 0 0 1 0 0 0 0 0 0 0 0 0 0 0 0 0 0 0 0 0 0 0
0 0 0 0 0 0;
      0 0 0 0 0 0 0 0 0 0 0 0 0 0 0 0 0 0 0 0 1 0 0
0 0 0 0 0 0];
k5_23=[kwb1 -kwb1;
      -kwb1 kwb1];
K5_23=T5_23'*k5_23*T5_23;

%DOF 7 Connects to DOF 27
%1 2 3 4 5 6 7 8 9 10 11 12 13 14 15 16 17 18 19 20 21 22 23 24
25 26 27 28 29 30
T7_27=[0 0 0 0 0 0 1 0 0 0 0 0 0 0 0 0 0 0 0 0 0 0 0 0
0 0 0 0 0 0;
      0 0 0 0 0 0 0 0 0 0 0 0 0 0 0 0 0 0 0 0 0 0 0
0 1 0 0 0 0];
k7_27=[kpm -kpm;
      -kpm kpm];
K7_27=T7_27'*k7_27*T7_27;

%DOF 9 Connects to DOF 23
%1 2 3 4 5 6 7 8 9 10 11 12 13 14 15 16 17 18 19 20 21 22 23 24
25 26 27 28 29 30
T9_23=[0 0 0 0 0 0 0 0 0 1 0 0 0 0 0 0 0 0 0 0 0 0 0 0
0 0 0 0 0 0;
      0 0 0 0 0 0 0 0 0 0 0 0 0 0 0 0 0 0 0 0 1 0 0
0 0 0 0 0 0];
k9_23=[kwb2 -kwb2;
      -kwb2 kwb2];
K9_23=T9_23'*k9_23*T9_23;

%DOF 11 Connects to DOF 28
%1 2 3 4 5 6 7 8 9 10 11 12 13 14 15 16 17 18 19 20 21 22 23 24
25 26 27 28 29 30
T11_28=[0 0 0 0 0 0 0 0 0 0 1 0 0 0 0 0 0 0 0 0 0 0 0 0
0 0 0 0 0 0 0;
      0 0 0 0 0 0 0 0 0 0 0 0 0 0 0 0 0 0 0 0 0 0 0
0 0 0 1 0 0];
k11_28=[kbn -kbn;
      -kbn kbn];
K11_28=T11_28'*k11_28*T11_28;

%DOF 15 Connects to DOF 29
%1 2 3 4 5 6 7 8 9 10 11 12 13 14 15 16 17 18 19 20 21 22 23 24
25 26 27 28 29 30

```

```

T15_29=[0 0 0 0 0 0 0 0 0 0 0 0 0 0 1 0 0 0 0 0 0 0 0 0
0 0 0 0 0 0 0;
        0 0 0 0 0 0 0 0 0 0 0 0 0 0 0 0 0 0 0 0 0 0 0 0
0 0 0 0 1 0];
k15_29=[kbm -kbm;
        -kbm kbm];
K15_29=T15_29'*k15_29*T15_29;

%DOF 17 Connects to DOF 24
        %1 2 3 4 5 6 7 8 9 10 11 12 13 14 15 16 17 18 19 20 21 22 23 24
25 26 27 28 29 30
T17_24=[0 0 0 0 0 0 0 0 0 0 0 0 0 0 0 0 1 0 0 0 0 0 0 0
0 0 0 0 0 0 0;
        0 0 0 0 0 0 0 0 0 0 0 0 0 0 0 0 0 0 0 0 0 0 1
0 0 0 0 0 0 0];
k17_24=[kwb1 -kwb1;
        -kwb1 kwb1];
K17_24=T17_24'*k17_24*T17_24;

%DOF 19 Connects to DOF 24
        %1 2 3 4 5 6 7 8 9 10 11 12 13 14 15 16 17 18 19 20 21 22 23 24
25 26 27 28 29 30
T19_24=[0 0 0 0 0 0 0 0 0 0 0 0 0 0 0 0 0 1 0 0 0 0 0
0 0 0 0 0 0 0;
        0 0 0 0 0 0 0 0 0 0 0 0 0 0 0 0 0 0 0 0 0 0 1
0 0 0 0 0 0 0];
k19_24=[kwb2 -kwb2;
        -kwb2 kwb2];
K19_24=T19_24'*k19_24*T19_24;

%DOF 21 Connects to DOF 30
        %1 2 3 4 5 6 7 8 9 10 11 12 13 14 15 16 17 18 19 20 21 22 23 24
25 26 27 28 29 30
T21_30=[0 0 0 0 0 0 0 0 0 0 0 0 0 0 0 0 0 0 0 1 0 0 0
0 0 0 0 0 0 0;
        0 0 0 0 0 0 0 0 0 0 0 0 0 0 0 0 0 0 0 0 0 0 0
0 0 0 0 0 1];
k21_30=[kbm -kbm;
        -kbm kbm];
K21_30=T21_30'*k21_30*T21_30;

%Tires to Ground
%DOF 23 Connects to DOF 23
        %1 2 3 4 5 6 7 8 9 10 11 12 13 14 15 16 17 18 19 20 21 22 23 24
25 26 27 28 29 30
T23_23=[0 0 0 0 0 0 0 0 0 0 0 0 0 0 0 0 0 0 0 0 0 1 0
0 0 0 0 0 0 0];
K23_23=T23_23'*(kt1+kt2)*T23_23;

%DOF24 connects to DOF 24
        %1 2 3 4 5 6 7 8 9 10 11 12 13 14 15 16 17 18 19 20 21 22 23 24
25 26 27 28 29 30
T24_24=[0 0 0 0 0 0 0 0 0 0 0 0 0 0 0 0 0 0 0 0 0 0 1
0 0 0 0 0 0 0];

```

```

K24_24=T24_24'*(kt1+kt2)*T24_24;

%Internal Components
%Dof 25 Connects to Dof 26
    %1 2 3 4 5 6 7 8 9 10 11 12 13 14 15 16 17 18 19 20 21 22 23 24
25 26 27 28 29 30
T25_26=[0 0 0 0 0 0 0 0 0 0 0 0 0 0 0 0 0 0 0 0 0 0 0
1 0 0 0 0 0 0;
    0 0 0 0 0 0 0 0 0 0 0 0 0 0 0 0 0 0 0 0 0 0
0 1 0 0 0 0 0];
%10 PSF Solution
    k25_26_10PSF=[kc(1) -kc(1);
                  -kc(1) kc(1)];
K25_26_10PSF=T25_26'*k25_26_10PSF*T25_26;

%20 PSF Solution
k25_26_20PSF=[kc(2) -kc(2);
              -kc(2) kc(2)];
K25_26_20PSF=T25_26'*k25_26_20PSF*T25_26;

%30 PSF Solution
k25_26_30PSF=[kc(3) -kc(3);
              -kc(3) kc(3)];
K25_26_30PSF=T25_26'*k25_26_30PSF*T25_26;

%40 PSF Solution
k25_26_40PSF=[kc(4) -kc(4);
              -kc(4) kc(4)];
K25_26_40PSF=T25_26'*k25_26_40PSF*T25_26;

%50 PSF Solution
k25_26_50PSF=[kc(5) -kc(5);
              -kc(5) kc(5)];
K25_26_50PSF=T25_26'*k25_26_50PSF*T25_26;

%60 PSF Solution
k25_26_60PSF=[kc(6) -kc(6);
              -kc(6) kc(6)];
K25_26_60PSF=T25_26'*k25_26_60PSF*T25_26;

%Dof 28 Connects to Dof 29
    %1 2 3 4 5 6 7 8 9 10 11 12 13 14 15 16 17 18 19 20 21 22 23 24
25 26 27 28 29 30
T28_29=[0 0 0 0 0 0 0 0 0 0 0 0 0 0 0 0 0 0 0 0 0 0
0 0 0 1 0 0 0;
    0 0 0 0 0 0 0 0 0 0 0 0 0 0 0 0 0 0 0 0 0 0
0 0 0 0 1 0 0];
k28_29=[kb -kb;
        -kb kb];
K28_29=T28_29'*k28_29*T28_29;

%Dof 29 Connects to Dof 30
    %1 2 3 4 5 6 7 8 9 10 11 12 13 14 15 16 17 18 19 20 21 22 23 24
25 26 27 28 29 30

```

```

T29_30=[0 0 0 0 0 0 0 0 0 0 0 0 0 0 0 0 0 0 0 0 0 0 0 0
0 0 0 0 1 0;
        0 0 0 0 0 0 0 0 0 0 0 0 0 0 0 0 0 0 0 0 0 0 0
0 0 0 0 0 1];
k29_30=[kb -kb;
        -kb kb];
K29_30=T29_30'*k29_30*T29_30;

```

```

K_EOM_10PSF=K1_25 + K3_26 + K5_23 + K7_27 + K9_23 + K11_28 + K15_29 +
K17_24 + K19_24 + K21_30 + K23_23 + K24_24 + K25_26_10PSF + K28_29 +
K29_30;
K_EOM_20PSF=K1_25 + K3_26 + K5_23 + K7_27 + K9_23 + K11_28 + K15_29 +
K17_24 + K19_24 + K21_30 + K23_23 + K24_24 + K25_26_20PSF + K28_29 +
K29_30;
K_EOM_30PSF=K1_25 + K3_26 + K5_23 + K7_27 + K9_23 + K11_28 + K15_29 +
K17_24 + K19_24 + K21_30 + K23_23 + K24_24 + K25_26_30PSF + K28_29 +
K29_30;
K_EOM_40PSF=K1_25 + K3_26 + K5_23 + K7_27 + K9_23 + K11_28 + K15_29 +
K17_24 + K19_24 + K21_30 + K23_23 + K24_24 + K25_26_40PSF + K28_29 +
K29_30;
K_EOM_50PSF=K1_25 + K3_26 + K5_23 + K7_27 + K9_23 + K11_28 + K15_29 +
K17_24 + K19_24 + K21_30 + K23_23 + K24_24 + K25_26_50PSF + K28_29 +
K29_30;
K_EOM_60PSF=K1_25 + K3_26 + K5_23 + K7_27 + K9_23 + K11_28 + K15_29 +
K17_24 + K19_24 + K21_30 + K23_23 + K24_24 + K25_26_60PSF + K28_29 +
K29_30;

```

```

%COMPLETE SYSTEM MASS AND SPRING MATRIX
M_system_10PSF=blkdiag(M_Frame, M_EOM_10);
M_system_20PSF=blkdiag(M_Frame, M_EOM_20);
M_system_30PSF=blkdiag(M_Frame, M_EOM_30);
M_system_40PSF=blkdiag(M_Frame, M_EOM_40);
M_system_50PSF=blkdiag(M_Frame, M_EOM_50);
M_system_60PSF=blkdiag(M_Frame, M_EOM_60);

```

```

K_system_10PSF=K_EOM_10PSF+k_ver30;
K_system_20PSF=K_EOM_20PSF+k_ver30;
K_system_30PSF=K_EOM_30PSF+k_ver30;
K_system_40PSF=K_EOM_40PSF+k_ver30;
K_system_50PSF=K_EOM_50PSF+k_ver30;
K_system_60PSF=K_EOM_60PSF+k_ver30;

```

```

%defining Damping of the system
C_system_10PSF=0.0001*K_system_10PSF+0.05*M_system_10PSF;
C_system_20PSF=0.0001*K_system_20PSF+0.05*M_system_20PSF;
C_system_30PSF=0.0001*K_system_30PSF+0.05*M_system_30PSF;
C_system_40PSF=0.0001*K_system_40PSF+0.05*M_system_40PSF;
C_system_50PSF=0.0001*K_system_50PSF+0.05*M_system_50PSF;
C_system_60PSF=0.0001*K_system_60PSF+0.05*M_system_60PSF;

```

```

%Eigenvalues 10PSF
[V_10PSF,lambda_10PSF]=eig(K_system_10PSF,M_system_10PSF);
omega_10PSF=(lambda_10PSF.^0.5)/(2*pi);

%Eigenvalues 20PSF
[V_20PSF,lambda_20PSF]=eig(K_system_20PSF,M_system_20PSF);
omega_20PSF=(lambda_20PSF.^0.5)/(2*pi);

%Eigenvalues 30PSF
[V_30PSF,lambda_30PSF]=eig(K_system_30PSF,M_system_30PSF);
omega_30PSF=(lambda_30PSF.^0.5)/(2*pi);

%Eigenvalues 40PSF
[V_40PSF,lambda_40PSF]=eig(K_system_40PSF,M_system_40PSF);
omega_40PSF=(lambda_40PSF.^0.5)/(2*pi);

%Eigenvalues 50PSF
[V_50PSF,lambda_50PSF]=eig(K_system_50PSF,M_system_50PSF);
omega_50PSF=(lambda_50PSF.^0.5)/(2*pi);

%Eigenvalues 60PSF
[V_60PSF,lambda_60PSF]=eig(K_system_60PSF,M_system_60PSF);
omega_60PSF=(lambda_60PSF.^0.5)/(2*pi);

%Natural Frequencies for the Beam
[V_Frame,lambda_Frame]=eig(K_Frame,M_Frame);
omega_Frame=(lambda_Frame.^0.5)/(2*pi);

%Plot Mode Shapes

for ii=1:10
    figure
    plot_truck_FE(V_60PSF(:,ii))
    title(sprintf('Mode Shape # %d Wn= %x Hz',ii,omega_60PSF(ii,ii)))
end

% Define frequency and time
freq=[0:0.5:80]'; % Hz
omega=2*pi*freq; % rads/sec
time=[0:0.001:2]'; % time

%*****Begin Powertrain input
%Firing Frequency RPSec * Engine Order
FF_6=(900/60)*3; %RPM convert to RPS * Engine Order

%Idle 1800 RPM engine order 3 (6 Cylinders)-Forcing Function
Fp_6=10*(1-0.1*(FF_6-freq).*(FF_6-freq));
Fp_6(find(Fp_6<0.0001))=0.0001;

%*****END OF Powertrain input

%*****Begin Road Input

```



```

hold all
plot (freq, (180/pi)*angle(x25_23))
plot (freq, (180/pi)*angle(x25_24))
xlabel('Frequency (Hz)')
ylabel('Phase (degrees)')
subplot(2,1,1)
semilogy(freq,abs(x25_27_6))
hold all
semilogy(freq,abs(x25_23))
semilogy(freq,abs(x25_24))
xlabel('Frequency (Hz)')
ylabel('Acceleration (m/s^2)')
legend('PTinput','Front Tire Input', 'Rear Tire Input')
title('Steering Column Excitation (DOF 25)');

%Plot magnitude and phase Steering Column (Acceleration)
figure
subplot(2,1,2)
plot(freq,(180/pi)*angle(x26_27_6))
hold all
plot (freq, (180/pi)*angle(x26_23))
plot (freq, (180/pi)*angle(x26_24))
xlabel('Frequency (Hz)')
ylabel('Phase (degrees)')
subplot(2,1,1)
semilogy(freq,abs(x26_27_6))
hold all
semilogy(freq,abs(x26_23))
semilogy(freq,abs(x26_24))
xlabel('Frequency (Hz)')
ylabel('Acceleration (m/s^2)')
legend('PTinput','Front Tire Input', 'Rear Tire Input')
title('Seat Excitation (DOF 26)');

%Plot magnitude and phase Steering Column (Displacement)
figure
subplot(2,1,2)
plot(freq,(180/pi)*angle(hd25_27))
hold all
plot (freq, (180/pi)*angle(hd25_24))
plot (freq, (180/pi)*angle(hd25_23))
xlabel('Frequency (Hz)')
ylabel('Phase (degrees)')
subplot(2,1,1)
semilogy(freq,abs(hd25_27))
hold all
semilogy(freq,abs(hd25_24))
semilogy(freq,abs(hd25_23))
xlabel('Frequency (Hz)')
ylabel('Displacement (m/N)')
title('Bode Plots for Half-Truck Model: Output Steering Column (DOF 25)')
legend('PTinput','Front Tire Input', 'Rear Tire Input')

```

```

%Plot magnitude and phase of Steering Column (Accleration)
figure
subplot(2,1,2)
plot(freq,(180/pi)*angle(h25_27))
hold all
plot (freq, (180/pi)*angle(h25_24))
plot (freq, (180/pi)*angle(h25_23))
xlabel('Frequency (Hz)')
ylabel('Phase (degrees)')
subplot(2,1,1)
semilogy(freq,abs(h25_27))
hold all
semilogy(freq,abs(h25_24))
semilogy(freq,abs(h25_23))
xlabel('Frequency (Hz)')
ylabel('Amplitude (m/s^2/N)')
title('Bode Plots for Half-Truck Model: Output Steering Column (DOF
25)')
legend('PTinput','Front Tire Input', 'Rear Tire Input')

%Plot magnitude and phase of Seat (Acceleration)
figure
subplot(2,1,2)
plot(freq,(180/pi)*angle(h26_27))
hold all
plot (freq, (180/pi)*angle(h26_24))
plot (freq, (180/pi)*angle(h26_23))
xlabel('Frequency (Hz)')
ylabel('Phase (degrees)')
subplot(2,1,1)
semilogy(freq,abs(h26_27))
hold all
semilogy(freq,abs(h26_24))
semilogy(freq,abs(h26_23))
xlabel('Frequency (Hz)')
ylabel('Amplitude (m/s^2/N)')
title('Bode Plots for Half-Truck Model: Output Seat(DOF 26)')
legend('PTinput','Front Tire Input', 'Rear Tire Input')

%Plot magnitude and phase of Seat (Acceleration)
figure
subplot(2,1,2)
plot(freq,(180/pi)*angle(h27_27))
hold all
plot (freq, (180/pi)*angle(h27_24))
plot (freq, (180/pi)*angle(h27_23))
xlabel('Frequency (Hz)')
ylabel('Phase (degrees)')
subplot(2,1,1)
semilogy(freq,abs(h27_27))
hold all
semilogy(freq,abs(h27_24))
semilogy(freq,abs(h27_23))

```

```
xlabel('Frequency (Hz)')  
ylabel('Amplitude (m/s^2/N)')  
title('Bode Plots for Half-Truck Model: Output Powertrain(DOF 27)')  
legend('PTinput','Front Tire Input', 'Rear Tire Input')
```

Appendix B

